8-2019

An Ex Vivo Model of Elastin Degradation in Porcine Carotid Arteries for the Study of Abdominal Aortic Aneurysms

Hannah Gore
Clemson University, hgore@g.clemson.edu

AN EX VIVO MODEL OF ELASTIN DEGRADATION IN PORCINE CAROTID ARTERIES FOR THE STUDY OF ABDOMINAL AORTIC ANEURYSMS

A Thesis
Presented to
the Graduate School of
Clemson University

In Partial Fulfillment
of the Requirements for the Degree
Master of Science
Bioengineering

---

by
Hannah Gore
August 2019

Accepted by:
Dr. Naren Vyavahare, Committee Chair
Dr. Jiro Nagatomi
Dr. Agneta Simionescu

ABSTRACT

Abdominal aortic aneurysms (AAA) are an area of dilation in the vessel that is greater than 3.0 cm in diameter or an area of the vessel that enlarged to greater than 50% of the vessel's original diameter[1,2,3]. AAA are generally asymptomatic and if ruptured, have a mortality rate of 78-83%[4]. AAA account for approximately 45,000 surgeries performed in the United States annually and are the 13th leading cause of death in the United States[1,2]. Alterations of two extracellular matrix proteins, elastin and collagen, are associated with the formation of abdominal aortic aneurysms[5]. AAA formation is marked by degradation of elastin and collagen induced by matrix metalloproteinases (MMPs) as well as a decrease in the amount of smooth muscle cells in the artery[4,5].

Elastase is the standard method of inducing an aneurysm in arterial tissue by breaking down the elastin fibers in the extracellular matrix. Numerous in vivo models have been published to induce the formation of an aneurysm using elastase, however there has yet to be model optimized in an ex vivo environment showing progressive AAA formation[6,7]. An optimal ex vivo model is advantageous in the hopes of advancing aneurysmal research by studying abdominal aortic aneurysms through organ culture. This optimal ex vivo model should be consistent with previous in vivo models; diminished elastin content and smooth muscle cells and show presence of MMPs. Additionally, this model should minimize death of native cells in order to recapitulate an in vivo response and investigate the relationship between elastin damage and calcification. Therefore, our lab aims to produce an ex vivo model of elastase-induced elastin degradation in porcine carotid arteries that minimizes death of native cells.

DEDICATION

To my parents, Michael and Kim Gore, for their unwavering support and encouragement. I would not be here without you both.

ACKNOWLEDGMENTS

I would first like to thank Dr. Naren Vyavahare for the opportunity to work on this research project, and for his support and encouragement throughout this endeavor. I would also like to thank my committee members, Dr. Jiro Nagatomi and Dr. Agneta Simionescu. In addition, I would like to thank Dr. John Eberth and Brooks Lane at the University of South Carolina School of Medicine for their feedback and support on this project.

I would also like to thank my lab members, Salphala Dhital, Ph.D., Tyler Gibson, Saketh Karamched, Rika Krisanarungson, Kate Magee, Vaideesh Parasaram, Ph.D., Dipasha Sinha, and Sherry Wang for their help and support throughout this project. I would specifically like to extend my immense thanks to Saketh Karamched and Vaideesh Parasaram, Ph.D. for teaching me many of the methods needed to complete this project and for their mentorship over the years. Additionally, I would like to thank everyone at the Godley Snell Animal Research Center, particularly Travis Pruitt, Jesse Privett, and Tina Parker for their help with the animal work.

Lastly, I would like to thank the Clemson University Department of Bioengineering for this opportunity to further my education.

TABLE OF CONTENTS

Table of Contents (Continued)

Page

Table of Contents (Continued)

Page

LIST OF TABLES

LIST OF FIGURES

List of Figures (Continued)

CHAPTER ONE

INTRODUCTION

Cardiovascular diseases (CVD) are the leading cause of death in the United States[8,9]. CVD are responsible for 1 out of every 4 deaths in the United States, accounting for over 610,000 deaths per year. Aortic aneurysms accounted for nearly 10,000 deaths in the United States in 2014 and contributed to over 17,000 deaths in 2009[9,10,11]. In studying potential therapies for these CVD and understanding disease pathology and mechanisms, we must first understand the anatomy and physiology.

1.1 Arterial System Anatomy and Physiology

The cardiovascular system is a complex system in living organisms consisting of the heart, blood vessels, and blood. The blood vessels of the cardiovascular system consist of arteries, arterioles, capillaries, venules, and veins[12]. The direction of blood flow is as follows: from arteries, to arterioles, to capillaries, to venules, and then to veins (Figure 1.1). Most blood vessels consist of three tunics: the tunica intima (innermost), tunica media (middle), and tunica adventitia (outer) (Figure 1.1)[13]. These three tunics are all composed of smooth muscle cells and varying amounts of collagen and elastin. The cellular makeup of these different tunics is determined based on the blood vessel's function in the body[12].

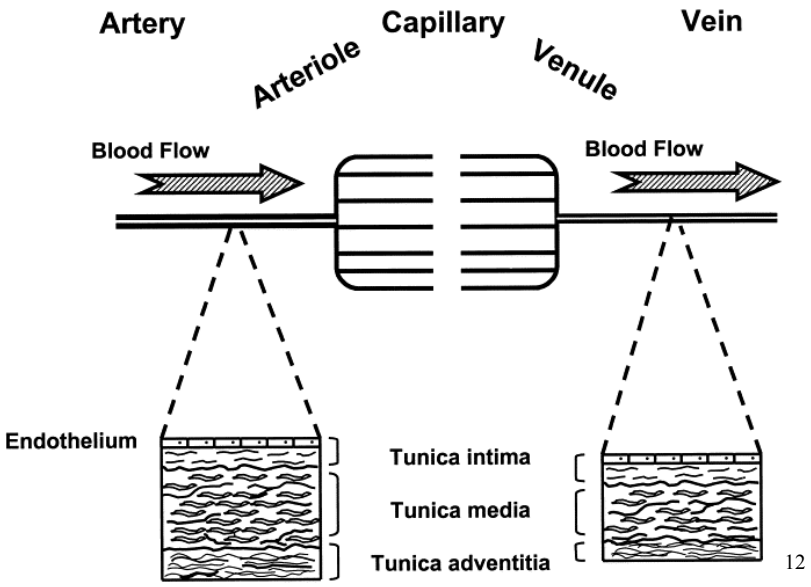

Figure 1.1: Direction of blood flow through the blood vessels and the three tunics of blood vessels[12].

The tunica intima is connected to a basement membrane and is composed of one layer of endothelial cells[12]. Endothelial cells aid in homeostatic functions of vascular tissues, and play a role in both inflammatory and immune responses. The internal elastic lamina that is below the basement membrane aids the endothelial cells of the tunica intima by providing flexibility and stability to these cells. In addition to endothelial cells, another cell type, pericytes, are also found in the tunica intima. Pericytes are believed to have numerous functions, as they are capable of differentiating into a wide range of different cell types, like fibroblasts and vascular smooth muscle cells (VSMCs)[14]. Additionally, pericytes aid in contraction of the blood vessel[14]. The middle tunic, the tunica media is composed of elastin fibers and smooth muscle cells[12]. In larger arteries, the cells of the tunica media are highly organized, due to their function in contractibility of the vessel

required for the movement of large quantities of blood. The internal and external elastic lamina of the tunica media imparts structural support to this tunic and separates it from the intima and adventitia respectively. The outermost tunic, the tunica adventitia is nearly completely composed of connective tissue that is fibro-elastic in nature[12]. The tunica adventitia provides mechanical support as well as houses the vasa vasorum, a network of small blood vessels, to provide nutrients to the vessel wall cells.

Arteries can be classified as being either elastic or muscular[12]. Found nearest the heart, elastic (conducting) arteries aid in the movement of large quantities of blood and have many layers of elastin, an extracellular matrix (ECM) component that gives blood vessels elasticity. These elastic arteries aid the muscular (distributing) arteries in creating blood flow that is more homogenized by working to dampen the large oscillations of blood flow. Muscular arteries are more muscular in composition. These arteries are shown to have numerous smooth muscle cells along with elastin fibers that are discontinuous in nature[12].

Arteries bifurcate, becoming smaller, and become arterioles, working to diminish the flow of blood from larger arteries in order to prevent capillary damage further down-stream[12]. Capillaries connect the arterial and venous systems. Capillaries lack smooth muscle cells and are composed of a single layer of endothelial cells, pericytes, and a basement membrane. Nutrient and solute exchange occurs at the capillary bed via hydrostatic and osmotic pressures. From the capillaries, blood will flow through the venules, which come together to form veins in order to return blood to the heart[12].

1.2 Aorta Anatomy and Physiology

The aorta is the largest blood vessel in the body, carrying oxygenated blood to the body from the left ventricle via the aortic valve and is broken down into the thoracic and abdominal aorta[15]. The thoracic aorta involves the ascending aorta, aortic arch, and descending aorta. The aortic arch branches into the left subclavian artery, left common carotid artery, and innominate artery, which further bifurcates into the right common carotid artery and the right subclavian artery. After the descending thoracic aorta, the abdominal aorta emerges as it passes under the aortic hiatus of the diaphragm and ends as it branches into the right and left iliac arteries, usually 2-3 cm below the umbilicus (Figure 1.2)[16].

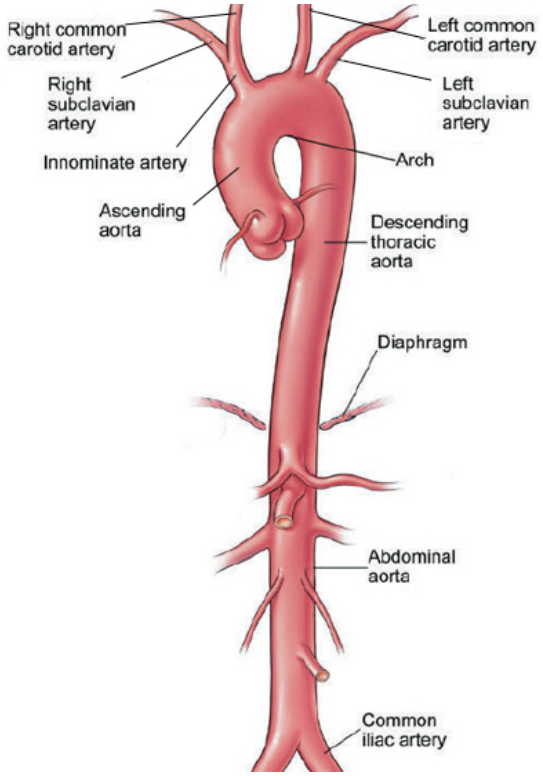

Figure 1.2: Anatomy of the aorta[17].

1.3 The Extracellular Matrix

The extracellular matrix (ECM) is a highly dynamic structure that is principally composed of polysaccharides, proteins, and water and is important in providing strength and stability to tissues, as well as being involved in cell adhesion, signaling, and differentiation[18,19]. The principle proteins of the ECM include proteoglycans and fibrous proteins, including collagens, elastin, and fibronectins.

1.3.1 Proteoglycans

Proteoglycans have glycosaminoglycan (GAG) chains that are linked by covalent bonds to a core protein[20]. Proteoglycans are found in the extracellular interstitial space of the tissue and have important functions in buffering, hydration, binding, and force-resistance[19]. GAGs are polymer chains that are linear and unbranched, consisting of repeating disaccharides that are composed of a hexosamine and a uronic acid[21]. GAGs have a negative charge, attracting Na^+, resulting in water migrating into the interstitial space of the ECM and causing the GAGs to swell as a result of the influx of water[21]. Thus, GAGs provide tissue hydration and compressive strength to the tissue.

1.3.2 Collagen

Of all the fibrous proteins in the ECM, collagen is the most abundant, forming one-third of the total protein in humans[21,22]. Collagen is a right-handed triple-helix held together by hydrogen bonds that are composed of XaaYaaGly resides, where the third residue must be Gly and Xaa and Yaa can be any amino acid[22]. (2S)-proline and 4-hydroxyproline are the amino acids most found in the Xaa and Yaa positions, respectively. Collagens serve important roles in cell adhesion, chemotaxis and cell migration, tissue development, and in providing tensile strength to the tissue. Collagen fibrils are formed by self-assembly[23]. Due to its ability to self-assemble and crosslink, collagen is important in providing strength and stability to the ECM[24]. Collagen is both transcribed and secreted by fibroblasts. The fibroblasts influence the alignment of collagen fibers, as these cells are able to organize collagen fibers into sheets[19]. There have been over 16 different types of collagen identified

all coming from a single ancestral gene[25,26]. Of these 16 different types, 80-90% of these belong to collagen types I, II, and III[26].

Type I collagen is the most abundant collagen in the body and is found in skin, tendon, bone, ligaments, dentin, and interstitial tissues[26]. Type II is found in the cartilage and vitreous humor. Type III is found in the skin, muscle, blood and blood vessels. Type I collagen has the form $[\alpha1(I)]_2\alpha2$, as it is composed of two $\alpha1$-type I chains and one $\alpha2$-chain, while types II and III have the forms $[\alpha1(II)]_3$ and $[\alpha1(III)]_3$, respectively, having three $\alpha1$-type II chains and three $\alpha1$-type III chains[27]. Type III collagen has been shown to be of great importance in maintaining the structural integrity of the blood vessels[28]. Though the association of type III collagen and blood vessels has been established, the molecular function of type III collagen in this regard is still largely unknown[28].

1.3.3 Elastin

Elastin fibers are important in providing recoil to tissues that are stretched repeatedly, examples being skin, lungs, blood vessels, and elastic cartilage. These elastin fibers are composed of elastin and microfibrils[29]. 90% of the composition of elastic fibers is elastin that is surrounded by microfibrils that are composed of numerous glycoproteins such as fibrillin and fibulins[30]. Elastin has minimal polar groups and numerous hydrophobic amino acid residues. Elastin is derived from its precursor, tropoelastin, and is highly cross-linked by lysine residues due to the action of lysyl oxidase enzymes that makes elastin an insoluble protein[17,31,32]. Lysyl oxidase cross-links elastin via the conversion of amine side chains in lysine residues to aldehydes[33]. Two additional amino

acid cross-linking residues of elastin are desmosine and isodesmosine, which are specific only for elastin and eggshell protein[33,34]. The ability of elastin to stretch is dictated by its association with collagen fibers[19]. Elastin can be degraded by proteases with elastase activity[3]. Figure 1.3 depicts the process of elastin formation and crosslinking, as derived from its precursor tropoelastin, and its degradation by the elastase enzyme[35].

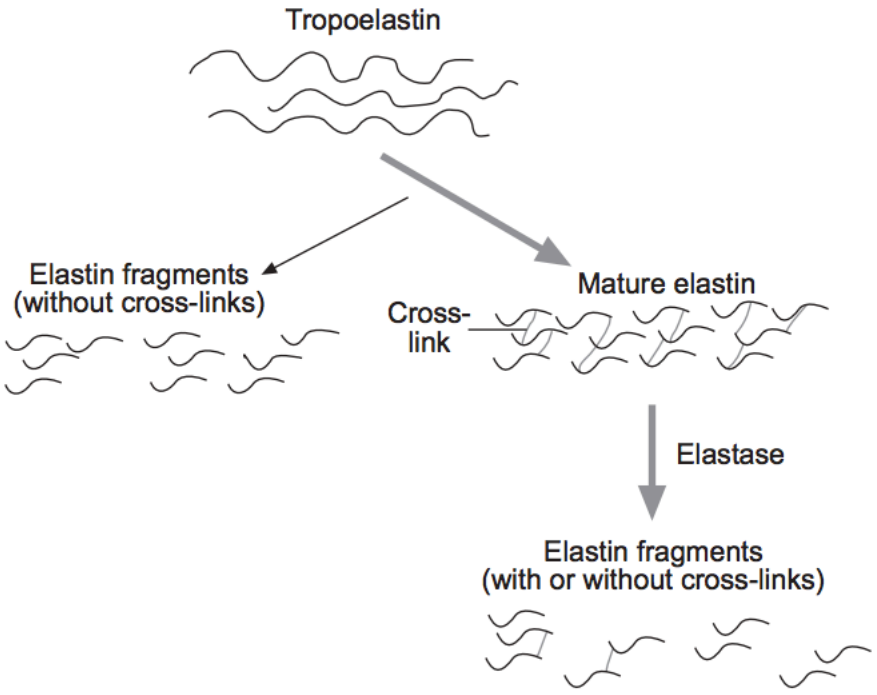

Figure 1.3: Mechanism of elastin formation from tropoelastin and degradation by elastase[35].

The structure and organization of elastin fibers varies throughout different tissues. These differences in are depicted in Figure 1.4. In arteries, elastic fibers are organized into rings within the lumen of the artery. In lung tissue, the organization of elastin fibers is

concentrated in areas of the organ like the alveoli that are exposed to high stress. When observed in elastic cartilage, the elastin fibers are found in a honeycomb like organization[30].

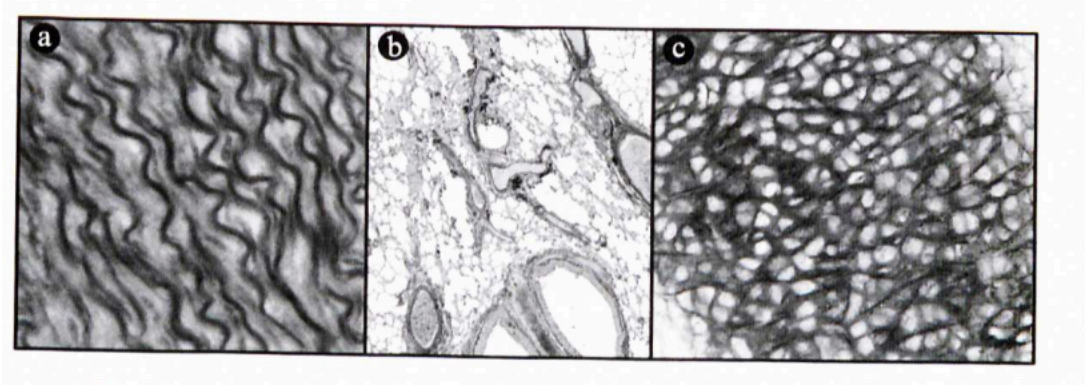

Figure 1.4: Elastin fiber organization in arteries (a), lungs (b), and elastic cartilage (c)[30].

1.3.4 Fibronectin

Fibronectin has important roles in ECM organization as well as in cell attachment and cell function. Fibronectin is a dimeric protein consisting of greater that 50 repeating subunits[36]. Fibronectin is an important mechanical regulator of the ECM, as this ECM protein can be stretched beyond its initial length, exposing integrin-binding sites which allow fibronectin to have roles in both scaffolding and cell recognition[36]. This ECM protein is implicated in the response to tissue injury, aiding in the formation of granulation tissue in the wound healing process[37].

1.4 Abdominal Aortic Aneurysm

1.4.1 Overview

Abdominal aortic aneurysms (AAA) are caused by expansion in the infrarenal portion of the aorta that leads to weakening of the arterial wall (Figure 1.5). This ballooning of the wall, caused by degeneration of the ECM components elastin and collagen can lead to ultimate rupture of the wall, causing significant blood loss that is fatal if not treated quickly. Clinically, AAA are characterized as an area of dilation in the vessel that is greater than 3.0 cm in diameter or an area of the vessel that is enlarged to greater than 50% of the vessel's original diameter[1,2,3]. A healthy infrarenal portion of the aorta has a diameter of 15-24 mm. In the event of AAA rupture, the mortality rate is 78-83%[38]. The prevalence of AAA is between 1.7-12.7% and AAA are currently the 13th leading cause of death in the United States[3,38]. AAA are typically asymptomatic, as around 75% of patients have no symptoms and are diagnosed through imaging performed for other health issues[39]. In patients that do experience symptoms, these symptoms are often relatively vague, including complaints of back and abdominal pain[3].

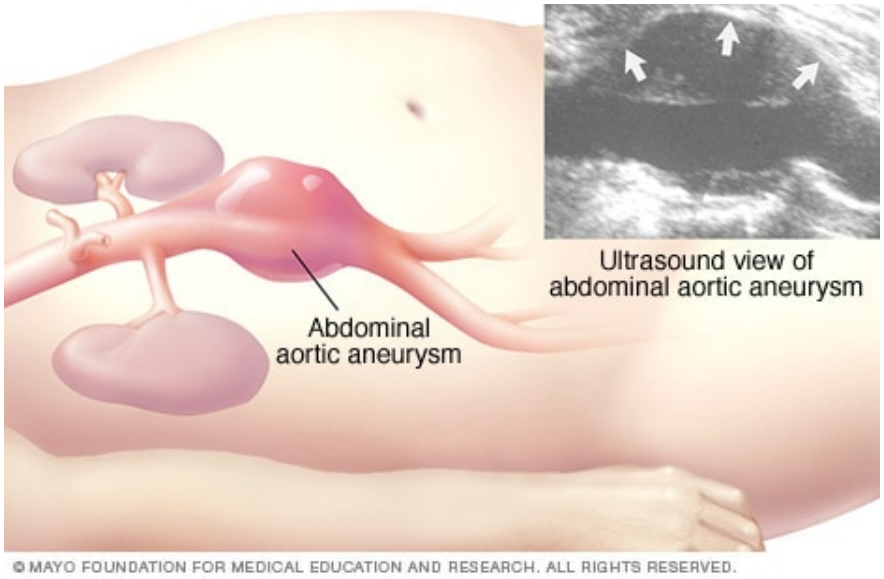

Figure 1.5: Abdominal aortic aneurysm[40].

1.4.2 Risk Factors

There are several risk factors associated with AAA. Caucasian men over age 60 are those that have the highest risk of having AAA, as 5-10% of men over the age of 65 will be diagnosed with AAA[3,39]. The cause of this gender disparity still remains largely unknown[41]. Elastase induced AAA models in rodents have shown a marked increase in male rodents (82%) forming AAA over females (29%). The male rodents showed an increase in the presence of MMP-9 secreting macrophages within the aorta[41].

Smoking is considered the risk factor with the strongest connection to the development of AAA. Years smoking is directly related to the risk of developing AAA; those who have an extensive history of smoking are more likely to develop a AAA than those with a less lengthy smoking history. Additionally, current smokers have a higher rate of expansion of their AAA compared to non-smokers; 2.83 mm growth annually in current

smokers and 2.53 mm growth annually in non-smokers. Though the association with smoking and increased risk of AAA formation has been discovered, the mechanism between the two has yet to be discovered.

Atherosclerosis is also a commonly associated risk factor with AAA. It is believed that the ECM remodels in response to shear stress alterations due to arterial stenosis, as elastin fibers in the ECM break due to the influx of inflammatory cells associated with stenosis[42]. Coronary artery disease is also a risk factor associated with AAA, as 40-60% of patients with AAA also have coronary artery disease, however the mechanisms associating the two conditions are still largely unknown[3,43].

Family history is also an important risk factor in AAA formation. Those that have a family history of AAA have a four-fold increase in the potential for AAA formation[3]. Additionally, those with a family history of AAA that do develop a AAA have a higher risk of AAA rupture earlier in life than those with no AAA family history[3]. Genome-wide scans of families with at least 2 family members with AAA have shown the possibility of a genetic cause of AAA, specifically associated with genes on chromosome 19q13 and 4q31[44]. Possible genes in these chromosomal regions include interleukin 15, endothelin receptor A, programmed cell death 5, and LDL receptor-related protein 3[44]. Replication of these gene studies have yielded inconsistent results. Several additional studies have also looked into the relationship of the C677 variant of the methylenetetrahydrofolate reductase gene as a possible genetic cause of AAA, however these have yielded inconsistent results as well[45,46,47,48].

1.4.3 Pathophysiology of AAA

AAA are marked by inflammation and increased production of proinflammatory cytokines, production of matrix-degrading proteinases, destruction of elastin and collagen in the ECM, diminished presence of vascular smooth muscle cells (VSMCs), and oxidative stress as depicted in Figure 1.6[49,50]. The mechanisms regarding the formation of AAA are still largely unknown, however the aforementioned markers can be used to confirm the presence of AAA histologically.

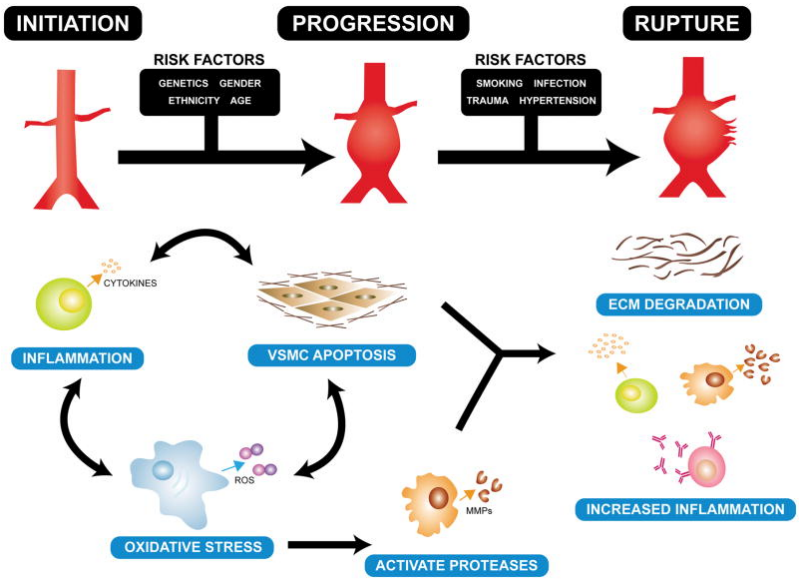

Figure 1.6: Pathogenesis of AAA[49].

Alteration of elastin and collagen in the ECM are strong markers to confirm the presence of AAA. Alteration of these ECM components is caused by the production of proteases by resident vascular cells like VSMCs, fibroblasts, and infiltrating inflammatory cells[3]. Matrix metalloproteinases (MMPs) are important in remodeling of the ECM and are

particularly involved in the turnover of both elastin and collagen[51]. MMPs all share a catalytic site that is zinc dependent, require Ca^{2+}, and are secreted by a latent proenzyme form. The primary activation of proteolytic enzymes is proceeded by cleavage of the propeptide by autocatylatic activation[52]. Two specific MMPs, MMP-2 and MMP-9 are implicated in the degradation of collagen and elastin, along with other substances and are associated with an inflammatory response caused by the invasion of macrophages[51,53]. MMP-2 (gelatinase A) is a 72 kDa protein produced from VSMCs located in the tunica media and tunica intima and from fibroblasts in the tunica adventitia. MMP-2 binding within the matrix is increased with the presence of AAA[52,53]. MMP-9 (gelatinase B) is a 92 kDa protein and is more abundant than MMP-2, as it is found in high levels in AAA due to its secretion by inflammatory cells, including neutrophils, macrophages, and macrophage-derived osteoclasts[52]. Elastin degradation due to MMPs is also associated with the onset of vascular calcification, however the mechanism remains unknown[54].

The diminished presence of VSMCs are thought to have implications in the capacity for repair of the ECM during this pathological process, further aiding in the formation of AAA[50]. VSMCs have roles in matrix synthesis, recruitment of inflammatory cells, and controlling proteases[55]. VSMC apoptosis has also been thought to initiate vascular calcification, as apoptotic blebs are able to collect calcium in a crystalized form[56]. Furthermore, these cells are elastolytic in AAA and believed to either have an acquired or innate phenotype that assists in degradation of the aorta due to the failure of a post-transcriptional control factor associated with MMP-9 synthesis, which increases the amount of MMP-9 activation in AAA[55].

Additionally, other enzymes including cathepsins have been implicated in degradation of collagen and elastin and associated with AAA[57]. Cathepsins are cysteine proteases regulated by pro-inflammatory stimuli. Cathepsin S is a potent elastase and cathepsin K is a potent collagenase, while cathepsin L has elastin and collagen degradation properties similar to cathepsin S and cathepsin K. Research has found that VSMCs within the tunica intima can create cathepsins S and K during AAA formation, suggesting that cathepsins play a role in ECM remodeling[58]. Cathepsins S, K, and L are expressed by macrophages and play a role in arterial wall rupture[57].

1.4.4 Current Treatments

Current treatment of AAA is determined based on the risk of rupture, procedure risk, and estimated life expectancy of the patient[2,3]. Currently, the size of the aneurysm is related to rupture risk, so patients with larger aneurysms are recommended for surgical treatment and those with aneurysms smaller than 5.5 cm are monitored by their physician as a more conservative approach without immediate surgical intervention, as studies have shown no benefit of early intervention for smaller aneurysms[59]. It is important to note that the rate of expansion of AAA after diagnosis is not related to the initial size of the aneurysm, so many believe that there are other factors associated with rate of expansion of the aneurysm.

Currently, there are two surgical options, open repair and endovascular repair which are depicted in Figure 1.7. During an open repair, a large incision is made from the distal aspect of the sternum, extending to the naval[60]. The aorta is exposed and the affected area

is clamped to stop blood flow. The aneurysm is located and a fabric graft is stitched into place, rerouting blood through the graft rather than through the weakened artery. The artery is then sutured closed. An endovascular repair is a minimally invasive surgical technique. During this procedure, a graft is guided to the aneurysmal potion of the artery using a catheter via the femoral artery, rerouting the blood flow through the graft rather than the weakened vessel wall[60].

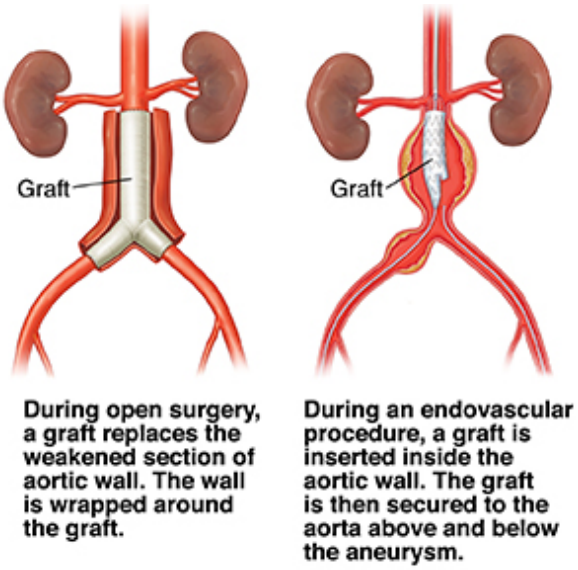

Figure 1.7: Comparison of an open AAA repair versus an endovascular AAA repair[61].

Studies have shown a diminished mortality rate within the first 30 days following surgery in an endovascular repair over an open repair; 1.6% versus 4.7%, respectively[59]. Despite the initial post-operative success, endovascular repairs are associated with increased post-operative complications and the need for reintervention later on. Additionally, there is no difference in quality of life after 3 months compared to an open

repair and there is no increase in survival compared to an open repair after 2 years[59]. The increased economic burden of an endovascular approach due to increased complications requiring possible reintervention and additional hospital stay, along with no significant differences in long term mortality and quality of life over time makes open repair the current gold standard for surgical repair of AAA.

1.5 Modeling AAA

Research continues to determine less invasive treatments for the prevention and treatment of AAA and further elucidate the mechanism of AAA formation[62].

1.5.1 In vitro Studies

Various groups have used cell culture methods to look for future methods to reverse elastin damage. Previous work from Kothapalli, et. al has shown the roles of hyaluronan (HA), transforming growth factor-ß1 (TGF- ß1), and insulin-like growth factor in elastogenesis and the how the coupling of HA and TGF- ß1 has shown increased VSMC proliferation and elastin synthesis and stability in healthy VSMCs[63,64,65]. This group looked into the roles of HA and TGF- ß1 in VSMCs extracted from diseased AAA tissues from rats 4 weeks after a periadvential application of calcium chloride to induce an aneurysm. They found that using HA and TGF- ß1 in concert were most effective, as there was significantly higher elastin synthesis through upregulation of lysyl oxidase and desmosine[66].

Additional work has been conducted to determine the possibility of the use of HA and TGF- ß1 to increase the elastogenic properties of VSMCs in late-stage AAA, where the VSMCs are unable to remodel damaged elastic fibers[67]. Aneurysmal rat SMCs (EaRASMCs) were harvested from adult male Sprangue Dawely rats 14 days after they underwent surgery to induce AAA formation via elastase perfusion. Supplementing HA and TGF- ß1in culture was shown to attenuate proliferation of EaRASMCs and increase synthesis of tropoelastin, while improving elastic fiber synthesis compared to healthy rat aortic SMCs (RASMCs). Additionally, supplementing HA and TGF- ß1 was found to restore the gene expression levels associated with EaRASMCs to mimic those associated with RASMCs. This study showed that it is possible to increase the elastogenic properties of SMCs in late-stage AAA via HA and TGF- ß1. One of the shortcoming of this approach was that there was no inhibition of MMP activity despite the incorporation of HA and TGF-ß1, thus newly formed elastin can further degrade and cause AAA[67].

Swaminathan et. al recently published their findings targeted at combating continued AAA growth by and reversing elastolysis[68]. This was done by optimizing the conditions for in situ regeneration of elastin using smooth muscle cells derived from rat bone marrow (BM-SMCs). Prior to this study, the same group had shown that BM-SMCs in high glucose conditions showed improved elastin fiber formation and reduced the presence of MMPs when compared to aneurysmal rat SMCs, predicating the need to further investigate the effects of phenotypic differences in BM-SMCs impact synthesis of the elastin matrix[69]. The group found that there was an intermediate SMC phenotype associated BM-SMCs in a low glucose environment supplemented with TGF- ß1 and platelet-derived

growth factor (PDGF-BB) that possessed increased tropoelastin and elastin matrix synthesis compared to controls[68].

Another group investigated the ways to mitigate high mobility group box 1 (HMGB1) production, which is produced by macrophages and associated with aortic inflammation and AAA formation[70]. They investigated the possibility of attenuating HMGB1 by coculturing macrophages from mice with mesenchymal stem cells (MSCs). A significant increase in HMGB1 was found in macrophages treated with elastase and this was diminished in macrophages cocultured with MSCs. Additionally, the study showed the association of nicotinamide adenine dinucleotide phosphate oxidase (Nox2) and HMGB1 production. There was a significant decrease in HMGB1 in elastase-treated macrophages from $Nox2^{-/y}$ mice and no significant decrease in HMGB1 when treated with cocultured with MSCs compared to the group solely treated with elastase. This lead to the conclusion that Nox2 plays a role in the production of HMGB1, thus helping to form AAA[70].

1.5.2 In vivo Studies

The most common ways to model AAA in animals involve continuous dosing of angiotensin II (Ang II) subcutaneously, subjecting the aorta to calcium chloride ($CaCl_2$) mediated perivascular injury, or a brief perfusion of elastase to the infrarenal aorta[71].

Ang II dosing is often used to study blood pressure alterations associated with atherosclerosis, however Ang II has also been shown to mimic the pathophysiology of AAA in humans through degradation of the elastic matrix, SMC apoptosis, oxidative stress,

and an inflammatory response[72,73]. The mechanism of AAA formation via Ang-II perfusion involves accumulation of macrophages followed by damage to elastin fibers and expansion of the vessel lumen with aortic remodeling and thrombus dissolution that is replaced by fibrous tissue and inflammatory cells[74].

Perivascular application of $CaCl_2$ to the infrarenal aorta also mimics the pathophysiology associated with AAA in humans including SMC apoptosis, oxidative stress, and degradation of the elastic matrix[75]. A pitfall to the $CaCl_2$ model are that it lacks aspects of human AAA pathophysiology including presence of atherosclerosis and aortic thrombus[75].

Of these three, elastase perfusion with porcine pancreatic elastase (PPE) is commonly used due to its ease of reproducibility, as the elastase is able to degrade the elastin fibers, subjecting the animal to AAA formation[76]. PPE is a serine protease that breaks down elastin[77]. It is a 240 amino acid long chain that begins with Val-16 and ends with Asn-245 and contains four disulfide bridges. PPE is inactive in the pancreas and is activated by trypsin when secreted into the intestines[77]. In murine animal models, the formation of AAA after elastase perfusion is thought to occur in two phases: the first being due to the loss of elastin fibers from the PPE perfusion, and the second resulting from an inflammatory response[78]. In the beginning days of this model, the elastin fibers become fragmented, followed by formation of a thrombus that accelerates AAA growth due to the activation and recruitment of MMP-2 and MMP-9[78].

Nosoudi et. al investigated the possibility of pentagalloyl glucose (PGG) loaded nanoparticles to protect elastin and prevent the development of AAA[79]. Mice were treated

perivascularly with $CaCl_2$ to form an aneurysm and PGG-loaded albumin nanoparticles were delivered through the tail vein 10 days following $CaCl_2$ mediated injury and sacrificed after 38 days. The PGG-loaded nanoparticles showed fewer macrophages in the tissue, a reduction in MMPs, less degradation of elastin, and aided in attenuating the formation of AAA[79,80].

The same group conducted a study on the use of a targeted nanoparticle therapy conjugated with a known MMP inhibitor, doxycycline to mitigate progression of AAA while providing no systemic side effects[81]. Previous research from the group showed the successful development of a targeted poly(D,L-lactide) nanoparticle that was conjugated with an antielastin antibody in rats that were targeted to the location of the elastin degradation in AAA. Expansion of this research included incorporating the MMP inhibitor batimastat (BB-94) within the previously constructed nanoparticles as a method to target the specific location of AAA in rats and preventing further growth of the aneurysm. AAA were induced in rats using a periarterial application of $CaCl_2$ and the drug loaded nanoparticles were delivered via the tail vein 10 days after AAA induction and continued weekly for 4 weeks. The results of the study showed that the nanoparticles successfully prevented MMP activity, degradation of elastin, calcification within the aorta, and prevention of AAA progression[81].

Studies have also been conducted to evaluate potential therapeutic treatments for AAA in animals by inhibiting necrosis induced by RIP3, a receptor-interacting protein kinase to determine if this inhibition has a significant effect on the progression of an established AAA[82]. AAA was induced in mice using elastase administration isolated within

the infrarenal aorta. Necrostatin-1 (Nec-1) and an optimized Nec-1, 7-Cl-O-Nec-1 (Nec-1s), both RIP1 inhibitors (RIP1 is closely related to RIP3) were delivered to the mice intraperitoneally 7 days after aneurysm induction and the mice were sacrificed at day 14[83]. The results showed a significant decrease in the aortic diameter of Nec-1s treated mice when compared to controls, histological results that were consistent with those of normal mice, and an increased amount of lysyl oxidase and tropoelastin within the aorta. Together, these results suggest the potential for a therapeutic approach using Nec-1s that prevents necrosis while providing stability to established AAA through a reduction in inflammation and increasing connective tissue repair[80,83].

The potential use of resolvins as a potential drug therapy for AAA has also been investigated[84]. Derived from docosahexaenoic acid, D-series resolvins are associated with resolution of inflammation in natural processes and have shown promise in various models of inflammatory diseases, inhibiting proinflammatory M1 macrophages and increasing anti-inflammatory M2 macrophages[84,85]. In a study investigating AAA treatment with the use of RvD2 and RvD1, two D-series resolvins, AAA were induced in mice by elastase perfusion and treated every 3rd day with an intraperitoneal injection of these resolvins until sacrifice and harvest of the aorta day 14. The results showed a 25% decrease in AAA size at day 14 in mice that received RvD2 injections compared to control mice. Additionally, histology confirmed the presence of M2 macrophages in the tissue of the RvD2 mice. The results of this study suggest that RvD2 is a possible treatment to halt AAA progression and that it is protected from the inflammatory response associated with aneurysms when administered after aneurysm formation[80,84].

Targeting focal adhesion kinase (FAK) has recently been studied as a potential drug therapy in slowing the expansion of AAA, as it has been associated with sustaining and intensifying inflammation associated with AAA[86]. After showing that FAK was necessary for AAA development in a $CaCl_2$ mouse model, mice were given PF573228, a FAK inhibitor after $CaCl_2$ dosage. PF573228 was either started at 3 weeks and given daily for 6 weeks, or at 3 weeks and only given for the following 4 days. The results showed that targeting FAK prevents progression of AAA, prevents MMP-9 activation, and diminishes recruitment of macrophages[80,86].

1.5.3 Organ Culture Studies

Wills, et. al exposed 1 cm sections of porcine thoracic aortas to concentrations of 1, 10, and 100 U/mL porcine pancreatic elastase (PPE) for 24 hours prior to being placed in standard medium and evaluated at time points of 1, 4, 9, and 14 days[87]. This study showed the progression of elastin damage over time and MMP presence. Additionally, in samples cultured with autogenous leukocytes, an inflammatory response was initiated, furthering the destruction of elastin and increasing MMP presence. The group was able to develop an organ culture model of AAA by identifying the presence of specific factors associated with AAA, including elastin damage, MMP presence, and an inflammatory response[87]. Pitfalls of this model include the failure to provide any evidence to prove that the dosage of elastase did not cause cell death or any histology to show if there was cell migration associated with the elastase dosage. Additionally, the quantitative analysis of VSMC concentration did show a decrease in concentration of VSMCs present over time

when compared to time-matched controls, however with the lack of histology, it is impossible to know if this is due to cell death from the PPE or VSMC apoptosis associated with AAA.

Since the publication of this paper, there has yet to be any further research in the development of an organ culture model of AAA. Because of this, a new organ culture model of progressive AAA formation is needed. This model should show elastin degradation and MMP presence like the Wills model, but should also show the cellular response to elastase dosage, providing a convincing progressive AAA model that mimics AAA pathophysiology in humans.

CHAPTER TWO

PROJECT RATIONALE

2.1 Overview

Current treatments for AAA involve invasive and risky procedures after a patient is deemed a surgical candidate[3]. Additionally, progression of small AAA in most patients is monitored by their physician. With conflicting options on how to predict the rupture risk of AAA, conservative monitoring could quickly turn deadly[2,3]. As the progression of research in AAA treatment and prevention strategies increases, additional models are needed for researchers to use to provide proof of concept before continued studies can be performed in humans.

At the moment, there has yet to be a successful organ culture model of AAA progression that shows the pathological features consistent with what is already known about AAA while maintaining cell viability[87]. Our lab plans to create an ex vivo organ culture model of AAA that minimizes cell death to fuel research for future AAA treatment methods.

This research will optimize the elastase concentration and dosage time to create a convincing progressive AAA organ culture model in fresh porcine carotid arteries. The successful development of this model will be confirmed using histological assessment of cell migration patterns, elastin damage, VSMC concentration, cell apoptosis, and MMP-2 and MMP-9 expression. This model will also investigate possible vascular calcification

associated with elastin damage. Additionally, desmosine content will be determined to provide further evidence of elastin damage and the relative fluorescence units (RFU) consistent with MMP-2 and MMP-9 presence will be used to further quantify MMP presence.

CHAPTER THREE

MATERIALS AND METHODS

3.1 Materials

The following chemicals and biologics were used for the research. Carotid arteries from female domestic crossbred pigs with a Yorkshire background (3-4 months old, 35-45 kg), sterile Moscona's solution (8 g NaCl, 0.2 g KCl, 1 g $NaHCO_3$, 1.7 g glucose, 0.005 g NaH_2PO_4 in 1 L DI water; pH 7.2), porcine pancreatic elastase (PPE) (Elastin Products Co., Inc., Owensville, MO), PPE buffer (100 mM Tris, 1mM $CaCl_2$, 0.02% NaN_3 in DI water; pH 7.8), frozen porcine carotid artery sections (Animal Technologies, Inc., Tyler, TX), high glucose serum free DMEM (GenDEPOT, Katy, TX), T-25 flasks (Corning Incorporated, Corning, NY), DMEM organ culture medium (high glucose DMEM, 10% FBS, 1% Penicillin/Streptomycin), 10% Neutral Buffered Formalin (Thermo Fisher Scientific, Waltham, MA), Tissue-TEK® tissue processor (Sakura Finetek USA, Inc., Torrance, CA), hematoxylin (Richard-Allen Scientific, San Diego, CA), permount mounting medium (Azer Scientific, Morgantown, PA), Motic BA210 light microscope (Motic, Hong Kong), Verhoeff van Gieson (VVG) staining kit (Poly Scientific R&D Corp., Bay Shore, NY), anti-alpha smooth muscle actin primary antibody (Novus Biologicals, Centennial, CO), citrate buffer (10 mM sodium citrate, 0.05% Tween 20; pH 6), goat anti mouse secondary antibody (Invitrogen, Rockford, IL), DAB peroxidase substrate (Vector, Burlingame, CA), TUNEL assay kit (Abcam, Cambridge, United Kingdom), RUNX2

antibody (Santa Cruz Biotechnology, Inc., Dallas, TX), normal horse serum (Vector, Burlingame, CA), avidin (Vector, Burlingame, CA), biotin (Vector, Burlingame, CA), ABC complex (Vector, Burlingame, CA), NovaRed peroxidase substrate (Vector, Burlingame, CA), OCT compound (Tissue-Tek®, Sakura Finetek USA, Inc., Torrance, CA), EVOS FL wide field fluorescent microscope, DAPI (ThermoScientific, Rockford, IL), DQ gelatin (Life Technologies Corporation, Eugene, OR), VECTASHIELD HardSet Antifade Mounting Medium with DAPI (Vector, Burlingame, CA), FRET (Fluorescence resonance energy transfer) Substrate III (Anaspec, Inc., Fremont, CA, Pierce™ BCA Protein Assay (ThermoScientific, Rockford, IL), porcine desmosine ELISA kit (MyBioSource, San Diego, CA).

3.2 Methods

3.2.1 Optimizing elastase dosage

Initially, elastase dosage was optimized in order to determine the ideal concentration and dosage time to induce elastin damage, observed via Verhoeff van Gieson staining (described in section 3.2.4.1.2) and without obvious cell death, observed via Hematoxlyin and Eosin staining (described in section 3.2.4.1.1).

Concentrations of 50U, 60U, and 80U of porcine pancreatic elastase (PPE) (Elastin Products Co., Inc., Owensville, MO) in PPE buffer (100 mM Tris, 1mM $CaCl_2$, 0.02% NaN_3 in DI water; pH 7.8) were applied to frozen carotid artery sections (Animal Technologies, Inc., Tyler, TX) and placed in a sterile incubator at 37°C and 5% CO_2 for 10

minutes and then washed in high glucose serum free DMEM (GenDEPOT, Katy, TX). Next, the sections were placed in 10% neutral buffered formalin and processed for histological analysis (described in section 3.2.4.1).

Additional optimization involved the use of concentrations of 10U and 20U of porcine pancreatic elastase (PPE) (Elastin Products Co., Inc., Owensville, MO) in PPE buffer (100 mM Tris, 1mM $CaCl_2$, 0.02% NaN_3 in DI water; pH 7.8) placed in a sterile incubator at 37°C and 5% CO_2 for time points of 20 minutes, 40 minutes, and 60 minutes and then washed in high glucose serum free DMEM (GenDEPOT, Katy, TX). Next, the sections were placed in 10% neutral buffered formalin and processed for histological analysis (described in section 3.2.4.1).

Upon histological analysis, the optimal concentration of elastase and dosage time was determined to be 20U of elastase for 15 minutes in a sterile incubator at 37°C and 5% CO_2 (further described in Chapters 4 and 5).

3.2.2 Obtaining fresh porcine carotid arteries

Following elastase optimization, fresh porcine carotid arteries were harvested from female domestic crossbred pigs with a Yorkshire background in Godley-Snell Research Center (Clemson, SC) for the following studies. All animals were 3-4 months old and weighed 35-45 kg. After the pigs were euthanized using commercial euthanasia solution, the thyroid cartilage was located. A 10 cm incision was made 3 cm laterally to the thyroid cartilage using a 10-blade scalpel, extending 5 cm superiorly to the thyroid cartilage and 5 cm inferiorly to the thyroid cartilage. Curved mayo scissors were used to dissect through

the underlying fascia and expose the sternocephalic muscle. The sternocephalic muscle was retracted to expose the internal and external jugular veins, the common carotid artery, and the vagus nerve. The carotid sheath was dissected using a 10-blade scalpel and the carotid artery was isolated and removed using surgical scissors. Following excision, the arteries were placed in sterile Moscona's solution (8 g NaCl, 0.2 g KCl, 1 g $NaHCO_3$, 1.7 g glucose, 0.005 g NaH_2PO_4 in 1 L DI water; pH 7.2) on ice and transported to the lab.

3.2.3 Elastase dosage

Upon return to the lab, the fat and adventitia surrounding the arteries were removed using fine-tip forceps. The carotid arteries were cut to 0.75 cm long sections using a 10-blade scalpel. Arteries were then subjected to a 20U dose of porcine pancreatic elastase (PPE) (Elastin Products Co., Inc., Owensville, MO) in PPE buffer (100 mM Tris, 1mM $CaCl_2$, 0.02% NaN_3 in DI water; pH 7.8). The artery was wrapped periarterially in sterile gauze absorbed with the elastase solution and placed in a sterile incubator at 37°C and 5% CO_2 for 15 minutes. The vessels were then washed in high glucose serum free DMEM (GenDEPOT, Katy, TX). After the washing step, the vessels were placed in T-25 flasks (Corning Incorporated, Corning, NY) with 15 mL DMEM organ culture medium (high glucose DMEM, 10% FBS, 1% Penicillin/Streptomycin) and placed in the sterile incubator at 37°C and 5% CO_2. The arteries were removed at 1, 3, and 7 days and placed in histology cassettes in 10% Neutral Buffered Formalin (Thermo Fisher Scientific, Waltham, MA).

3.2.4 Histology

Histological analysis was performed on the samples in order to investigate cell migration patterns, elastin fiber concentration and organization, VSMC apoptosis, MMP presence, and presence of calcification. Histological assessment was performed in control samples as well as samples that underwent elastase treatment as described previously.

3.2.4.1 Paraffin Sections

Following removal from culture, samples of 0.25 cm of tissue were put into tissue cassettes and fixed in 10% neutral buffered formalin for 24 hours. Following this initial fixation, the samples were processed in a Tissue-TEK® tissue processor (Sakura Finetek USA, Inc., Torrance, CA). Preparation of paraffin samples included immersion in formalin, increasing concentrations of ethanol, xylene, and finally infiltration in paraffin. After processing, the samples were embedded in paraffin wax and sectioned (6 μm sections), stained, and cover-slipped for analysis using a light microscope.

3.2.4.1.1 Hematoxylin and Eosin Staining (H&E)

Hematoxylin and Eosin (H&E) was performed on paraffin sections as a general stain to observe the extracellular matrix and the location of the cells within the tissue. The slides were first deparaffinized by dipping the slides in xylene for 10 dips, submerging the slides in xylene for 5 minutes, dipping the slides in 100% EtOH for 1 minute, submerging the slides in 100% EtOH for 1 minute, dipping the slides in 95% EtOH for 10 dips, submerging the slides in 95% EtOH for 1 minute, followed by rinsing the slides with tap

water until “sheeting” occurred, and then placed in distilled water for 1 minute. After deparaffinization, the slides were placed in hematoxylin (Richard-Allen Scientific, San Diego, CA) for 7 minutes and then rinsed in tap water until clear. Next, the slides were dipped in clarifier (Richard-Allen Scientific, San Diego, CA) 5 times, then dipped in tap water until a “sheeting” action occurred. The slides were then placed in bluing reagent (Richard-Allen Scientific, San Diego, CA) for 1 minute, placed in tap water for 1 minute, and dipped 10 times in 95% EtOH. The slides were then placed in eosin (Richard-Allen Scientific, San Diego, CA) for 35 seconds and dipped 10 times each through 2 cycles of 95% EtOH, 2 cycles of 100% EtOH, and 2 cycles of xylene. The slides remained in xylene until coverslipped with permount mounting medium (Azer Scientific, Morgantown, PA). The slides were finally imaged using a Motic BA210 light microscope (Motic, Hong Kong).

3.2.4.1.2 Verhoeff van Gieson Staining (VVG)

Verhoeff van Gieson (VVG) (Poly Scientific R&D Corp., Bay Shore, NY) staining was performed on paraffin sections to assess the quantity and organization of the elastin fibers within the vessel. The slides were first deparaffinized as described above. After deparaffinization, the slides were placed in Verhoeff’s Working Solution, prepared as directed by the supplier (5 mL Hematoxylin 5% Alcoholic solution, 2 mL Ferric Chloride 10% Aqueous, 2 mL Lugol’s Iodine Working Solution) and placed on the samples for 15 minutes. Following this, the slides were dipped in distilled water 10 times. The slides were then differentiated in Ferric Chloride 2% Aqueous for 20 seconds and then rinsed in tap

water. Sodium Thiosulfate 5% Aqueous was then placed on the slides for 1 minute and the slides were then washed in tap water for 5 minutes. Next, the slides were counterstained with Van Gieson's Solution for 3 minutes, rinsed with tap water briefly, allowed to dry, and coverslipped with permount mounting medium (Azer Scientific, Morgantown, PA). The slides were finally imaged using a Motic BA210 light microscope (Motic, Hong Kong).

3.2.4.1.3 IHC for VSMCs

IHC for detection of VSMCs was performed on paraffin sections using anti-alpha smooth muscle actin primary antibody (Novus Biologicals, Centennial, CO) in order to determine VSMC apoptosis. The slides were first deparaffinized as described above. After deparaffinization, the slides were heated in citrate buffer (10 mM sodium citrate, 0.05% Tween 20; pH 6) for 30 minutes at 95°C. The slides were then allowed to cool and were then washed in deionized water for 2 minutes. Following this, the slides were washed 3 times for 2 minutes each in IHC wash buffer (0.1 M PBS, 0.05% Tween; pH 7.4). The slides were then blocked with 3% H_2O_2 for 5 minutes and washed 3 times with IHC wash buffer for 2 minutes each. Non-specific binding blockage was then performed with 3% Bovine Serum Albumin (BSA) in PBS for 10 minutes and again washed 3 times with IHC wash buffer for 2 minutes each. The anti-alpha smooth muscle actin primary antibody (Novus Biologicals, Centennial, CO) was then placed on the samples and the samples were allowed to incubate overnight at 4°C; 0.1% BSA in PBS was used as a negative control for each sample.

After overnight incubation, the slides were washed 3 times with IHC wash buffer for 2 minutes each. Following this wash, a 1:500 dilution of goat anti mouse secondary antibody (Invitrogen, Rockford, IL) was placed on the samples for 1 hour at room temperature. The slides were then washed 3 times with IHC wash buffer for 2 minutes each. DAB peroxidase substrate (Vector, Burlingame, CA) was then prepared according to the manufacturer's directions and placed on the slides for 5 minutes followed by washing the slides with IHC wash buffer one time for 2 minutes.

Following the wash, the slides were stained with hematoxylin for 30 seconds, dipped through a series of alcohols as described previously, and coverslipped using permount mounting medium (Azer Scientific, Morgantown, PA). The slides were finally imaged using a Motic BA210 light microscope (Motic, Hong Kong).

3.2.4.1.4 TUNEL Assay

To observe apoptotic cells, a TUNEL assay was performed (Abcam, Cambridge, United Kingdom). The assay was performed according to the manufacture's recommendations, coverslipped using permount mounting medium (Azer Scientific, Morgantown, PA), and imaged using a Motic BA210 light microscope (Motic, Hong Kong).

3.2.4.1.5 Alizarin Red Staining

Alizarin red staining was performed to observe vascular calcification. Following deparrafinization as described previously, the slides were stained with 2% alizarin red

solution (pH 4.1-4.3) for 5 minutes. The slides were then dipped until clear in DI water and counterstained with 1% light green SF yellowish for 10 seconds and again dipped until clear in DI water. The slides were then dipped through a series of alcohols as described previously and coverslipped using permount mounting medium (Azer Scientific, Morgantown, PA). The slides were finally imaged using a Motic BA210 light microscope (Motic, Hong Kong).

3.2.4.1.6 IHC for RUNX2

IHC for detection of RUNX2, a transcription factor associated with osteoblast differentiation and one of the first markers of VSMC phenotypic switch to an osteogenic cell type was performed on paraffin sections using a RUNX2 antibody (Santa Cruz Biotechnology, Inc., Dallas, TX). The slides were first deparaffinized as described above. After this, the slides were boiled in citrate buffer (10 mM sodium citrate, 0.05% Tween 20; pH 6) for 10 minutes at 95°C. The slides were then allowed to cool. Following cooling, the slides were washed twice in IHC wash buffer (0.1 M PBS, 0.05% Tween; pH 7.4) for 5 minutes each. Non-specific binding blockage with normal horse serum (Vector, Burlingame, CA) was then performed for 40 minutes. The slides were then washed twice in IHC was buffer for 5 minutes each. Avidin (Vector, Burlingame, CA) was then placed on the slides for 15 minutes, followed by two 5 minute washes in IHC wash buffer. Next, biotin (Vector, Burlingame, CA) was plated on the slides for 15 minutes, followed by two 5 minute washes in IHC wash buffer. The RUNX2 primary antibody (Santa Cruz

Biotechnology, Inc., Dallas, TX) was then applied and the slides were kept overnight at 4°C; 0.1% BSA in PBS was used as a negative control for each sample.

Following overnight incubation, the slides were washed 2 times for 5 minutes each in IHC wash buffer. The slides were then blocked with 3% H_2O_2, for 10 minutes and then washed 2 times for 5 minutes each in IHC wash buffer. Following this wash, a 1:500 dilution of goat anti mouse secondary antibody (Invitrogen, Rockford, IL) was placed on the samples for 1 hour at room temperature. The slides were then washed in IHC wash buffer twice for 5 minutes each. ABC complex was then applied (Vector, Burlingame, CA) for 30 minutes followed by two 5 minute washes in IHC wash buffer. NovaRed peroxidase substrate (Vector, Burlingame, CA) was then prepared according to the manufacturer's directions and placed on the slides for 5 minutes followed by washing the slides with wash buffer one time for 5 minutes.

Following the wash, the slides were stained with hematoxylin 30 seconds, dipped through a series of alcohols as described previously, and coverslipped using permount mounting medium (Azer Scientific, Morgantown, PA). The slides were finally imaged using a Motic BA210 light microscope (Motic, Hong Kong).

3.2.4.2 Frozen Sections

Following removal from culture, 0.25 cm sections were cut, snap frozen in liquid nitrogen, and stored at -80°C until being prepared for cryosectioning. OCT compound (Tissue-Tek®, Sakura Finetek USA, Inc., Torrance, CA) was placed in molds and the samples were positioned within the OCT compound to be sectioned axially. The molds

were put into a reservoir containing acetone to act as a heat transfer agent and dropped in liquid nitrogen to freeze. The samples were kept at -80°C and sectioned with a cryosectioner (ThermoScientific, Waltham, MA) (6 um sections) before being stained, coverslipped, and imaged for analysis with an EVOS FL wide field fluorescent microscope.

3.2.4.2.1 In Situ Zymography

In situ zymography was performed to visualize MMP activity. Samples were air-dried for 10 minutes and stained with 1 ug/mL DAPI (ThermoScientific, Rockford, IL) for 2 minutes, followed by a 2 minute wash in deionized water. DQ gelatin (Life Technologies Corporation, Eugene, OR) was diluted 1:10 and placed in 2% (w/v) low gelling temperature agarose (Ambion, Inc., Foster City, CA) dissolved in deionized water. The mixture was placed on top of the slides and gelled at 4°C. After gelling, the slides were placed in development buffer (50 mM Tris Base, 5 mM $CaCl_2$*$2H_2O$, 200 mM NaCl, 0.02% brij 35; pH 7.6) overnight at 37°C. The slides were then coverslipped with VECTASHIELD HardSet Antifade Mounting Medium with DAPI (Vector, Burlingame, CA) and imaged with an EVOS FL wide field fluorescent microscope. Fluorescence of FITC (fluorescein isothiocyanate) was observed at an excitation of 460-500 nm and emission of 512-542 nm. DAPI was observed at an excitation of 340-380 nm and emission of 425-∞ nm.

3.2.5 Relative Fluorescence Units (RFU) for MMPs

Relative fluorescence units for MMPs were determined using extracted proteins from the samples. Following removal from culture, samples were cut into 0.2 mm sections

and kept at -80°C until protein extraction. To extract proteins, the samples were cut into small pieces, placed in 0.5 mL RIPA buffer (50 mM Tris-HCl, 150 mM NaCl, 1% Triton X-100, 1% sodium deoxycholate, 0.1% SDS; pH 7.4) and homogenized with a tissue homogenizer (Fisher Scientific, Hampton, NH) until completely dissolved. The samples were then centrifuged at 10,000 rpm for 5 minutes. Following this, the supernatant was saved. 96 uL of substrate buffer (50 mM Tris buffer, 5 mM CaCl2, 200 mM NaCl, 0.02% brij-35; pH 7.5), 2 uL 360 MMP FRET (Fluorescence resonance energy transfer) Substrate III (Anaspec, Inc., Fremont, CA), and 2 uL of the supernatant was added to a black 96-well plate (Fisherbrand, Pittsburgh, PA) and read (excitation 280 nm, emission 360 nm) using a plate reader (BioTek, Winooski, VT).

A Pierce™ BCA Protein Assay (ThermoScientific, Rockford, IL) was performed. A solution of Reagents A and B was created according to the manufacturer's directions, and 200 uL of this mixture was added to a mixture of 5 uL of supernatant and 5 uL of DI water in a clear 96-well plate (Fisherbrand, Pittsburgh, PA), incubated at 37°C for 20 minutes and read at an absorbance value of 562 nM using a plate reader (BioTek, Winooski, VT). Known standards of varying protein concentrations were also used in order to create a standard curve. From the results of the BCA assay, the absorbance values from the FRET assay were divided by the mg protein per sample detected from the BCA assay, and the amount of relative fluorescence units/mg protein were able to be calculated.

3.2.6 Desmosine ELISA

The amount of desmosine in each sample was determined using a porcine desmosine ELISA kit (MyBioSource, San Diego, CA). Following removal from culture, 0.2 cm sections were cut, snap frozen in liquid nitrogen, and stored at -80°C until being prepared for ELISA. The samples were placed in a lyphilizer (Labconco, Kansas City, MO) overnight and their dry weights were recorded. Following this, the samples were cut into small pieces and boiled in 0.5 mL 6N HCl at 95°C until dissolved. The samples were then dried with nitrogen gas under a laminar flow hood until the liquid was evaporated. 0.25 mL 0.1N HCl was used to resuspend the samples. ELISA was then performed according to the manufacturer's instructions. A standard curve was created with known samples and used to determine the amount of desmosine (ng desmosine/mg dry tissue) along with the recorded dry weights of the samples.

CHAPTER FOUR

RESULTS

4.1 Elastase Optimization

Initial attempts were made to determine how increasing concentrations of elastase affect elastin damage at a single time point. VVG staining showed that increasing concentrations (50U, 60U, and 80U) of PPE all applied for 10 minutes did not show an obvious change in elastin damage (Figure 4.1).

Lower concentrations (10U and 20U) of PPE applied at increasing time points (20 minutes, 40 minutes, and 60 minutes) showed that there was elastin damage present in the group treated with 20U of PPE for 60 minutes (Figure 4.2). While there was elastin damage seen with this dosage at days 1, 3, and 7 (Figure 4.3), H&E staining of the same samples revealed that there was an overwhelming amount of cell death (Figure 4.4), making a 20U dose for 60 minutes an unviable option for this model.

The use of 20U of PPE for 15 minutes was found to be the elastase dosage that worked to insure elastin damage, as well as minimize cell death and was the concentration and dosage time used for this model (Figures 4.5 and 4.6).

4.2 Histology

4.2.1 Hematoxylin and Eosin (H&E)

H&E staining showed that the cells migrated from the adventitial layer of the artery, where the elastase was applied, towards the lumen beginning at day 1 in the elastase-treated group. This is not seen in any of the control groups. Of note, it appears that the cells begin to migrate back from the lumen to the adventitial layer of the artery at day 7. Because of this observation, the model was extended to include a 14 day time point, however the H&E staining revealed cell death in the day 14 elastase treated group (Figure 4.5).

4.2.2 Verhoeff van Gieson (VVG)

VVG staining was performed to analyze the organization and deterioration of elastin fibers within the vessels. VVG staining stains elastin fibers black within the yellow/brown stained tissue. The elastin fibers appear numerous and organized in all control samples and at days 0 and 1. At day 3, the elastin fibers appear to be less thickly clustered and breaks are seen around the adventitial layer of the artery where the elastase was administered. This is also seen at day 7, with less elastin fibers located within the periphery of the artery than at day 3. Elastin damage is also observed in the day 14 elastase treated group, however since H&E staining revealed abundant cell death in this group, this model proceeded to evaluate samples at time points of 0, 1, 3, and 7 days (Figure 4.6).

4.2.3 IHC anti alpha-smooth muscle actin

Immunohistochemistry was performed for VSMC status using the anti alpha-smooth muscle actin antibody. There is a dramatic decrease in staining for SMC actin consistent with the loss of VSMCs as time progresses, particularly at day 7 (Figure 4.7).

4.2.4 TUNEL Assay

A TUNEL assay was performed to assess the presence of apoptotic cells within the samples. The Terminal deoxynucleotidyl Transferase (TdT) enzyme used in the assay binds to the exposed 3'-OH ends of DNA present in apoptotic cells and adds biotin-labeled deoxynucleotides that are further labeled with a streptavidin-horseradish peroxidase (HRP). This complex then reacts with DAB, which stains apoptotic cells brown. The images showed the presence of apoptotic cells at day 7 (Figure 4.8). The presence of these apoptotic cells were not seen in the control sample at the same time point or any time point, confirming that the apoptosis was due to the elastase dosage and not due to contamination in organ culture.

4.2.5 Alizarin Red

Alizarin red staining was performed to search for the presence of vascular calcification. The staining showed no calcification in any of the samples (Figure 4.9).

4.2.6 IHC RUNX2

Immunohistochemistry was performed for RUNX2, a transcription factor associated with osteoblast differentiation and one of the first markers of VSMC phenotypic switch to an osteogenic cell type was performed using the RUNX2 antibody. The images showed the presence of this transcription factor only in the day 7 elastase treated group, suggesting the early stages of VSMC phenotypic switch to an osteogenic cell type (Figure 4.10).

4.2.7 In situ Zymography

In situ zymography with DQ gelatin was performed to observe the presence and location of MMP-2 and MMP-9 within the samples. DQ gelatin in the gel is degraded by MMPs present in the tissue lysate and provides green fluorescence. DAPI stains cell nuclei blue. The results of the in situ zymography showed no visible presence of MMP-2 and MMP-9 in the control samples used at any time point nor in the day 0 elastase treated group. A small amount of green fluorescence was seen in the elastase treated group at day 1 (Figure 4.11). As time progresses, a marked increase in green fluorescence was observed consistent with increased MMP-2 and MMP-9 activity in the elastase treated groups at day 3 and day 7. It appears that the green fluorescence is most intense in the elastase treated group at day 3, suggesting that MMP activity peaks at day 3.

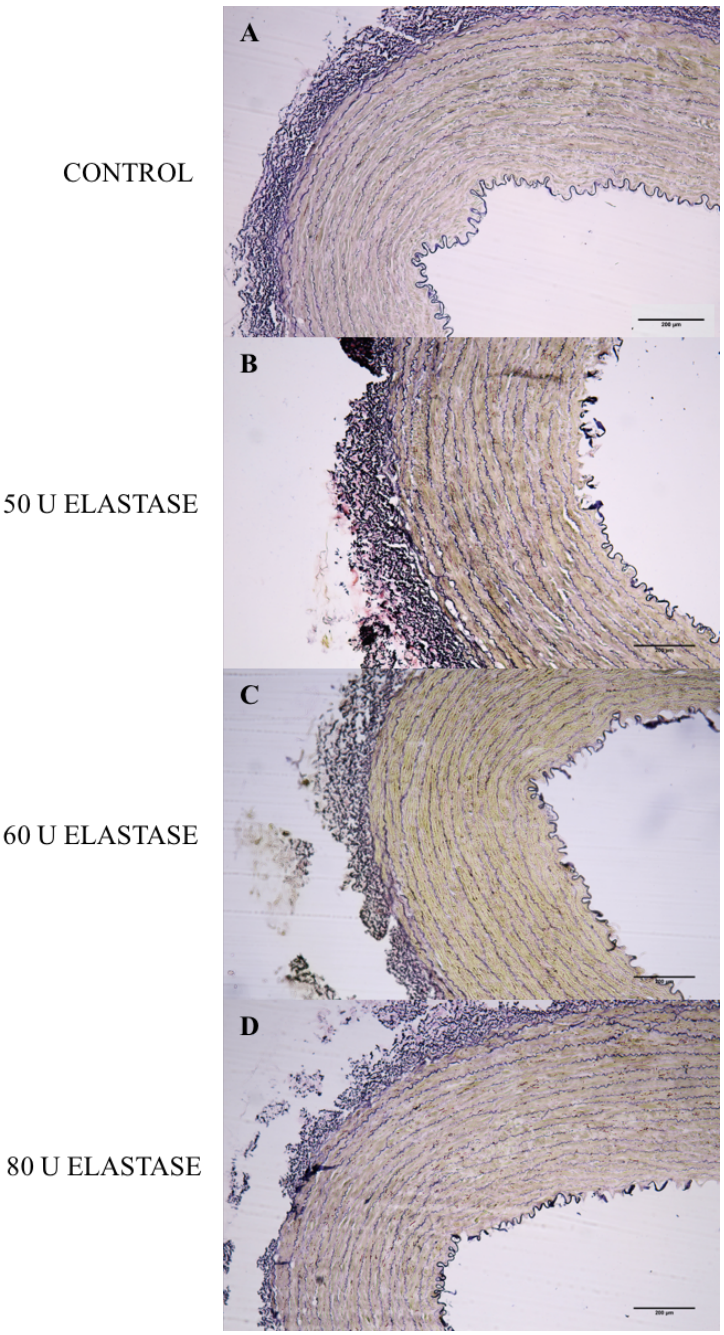

Figure 4.1: Verhoeff van Gieson (VVG) staining showing representative images (n = 3) of elastin damage in porcine carotid arteries; (A) control, 10 minutes; (B) 50U elastase, 10 minutes; (C) 60U elastase, 10 minutes; (D) 80U elastase, 10 minutes. 10x magnification.

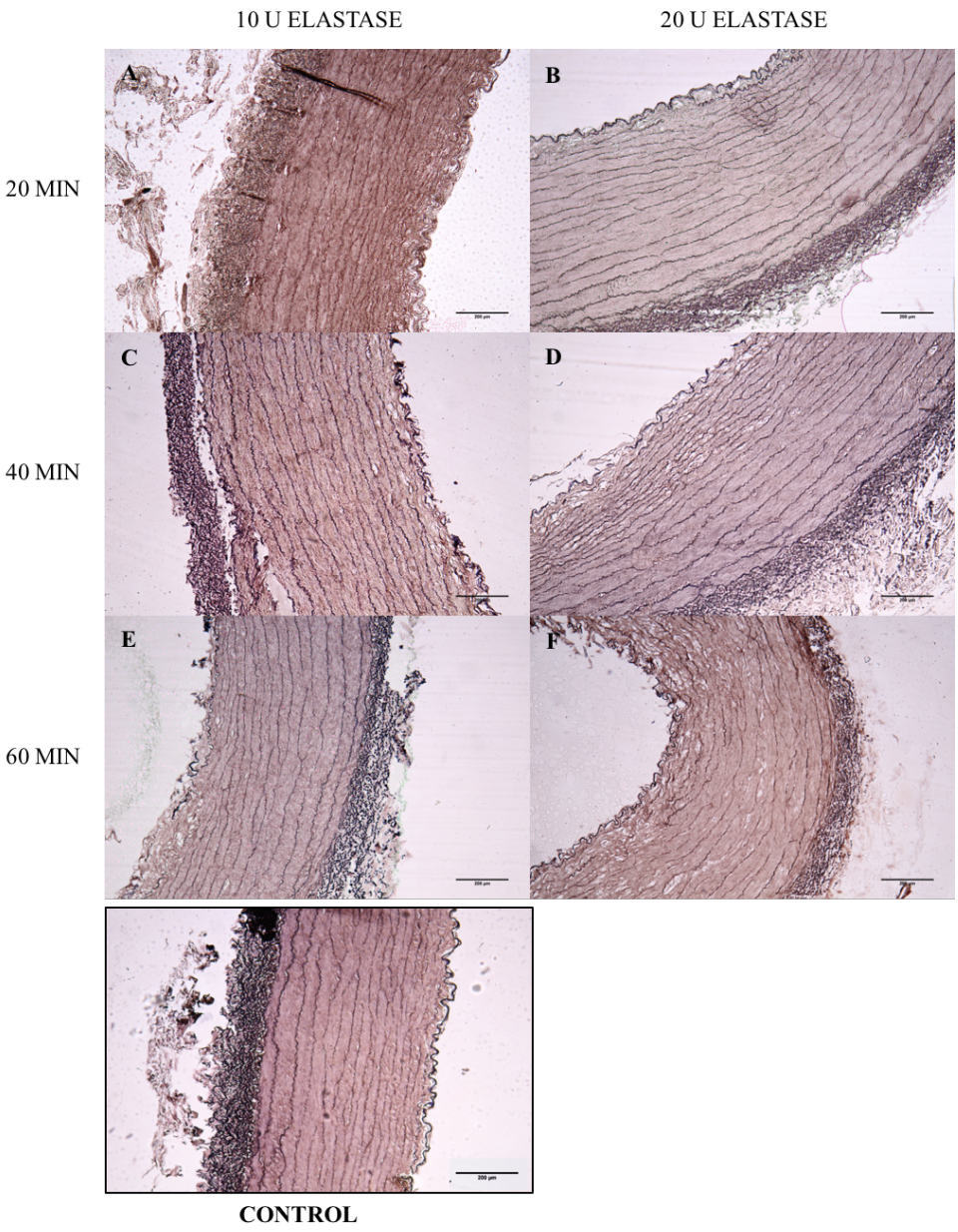

Figure 4.2: Verhoeff van Gieson (VVG) staining showing representative images (n = 3) of elastin damage in porcine carotid arteries; (A) 20U elastase, 20 minutes; (B) 20U elastase, 20 minutes; (C) 10U elastase, 40 minutes; (D) 20U elastase, 40 minutes; (E) 10U elastase, 60 minutes; (F) 20U elastase, 60 minutes. Control shown in bottom left corner. 10x magnification.

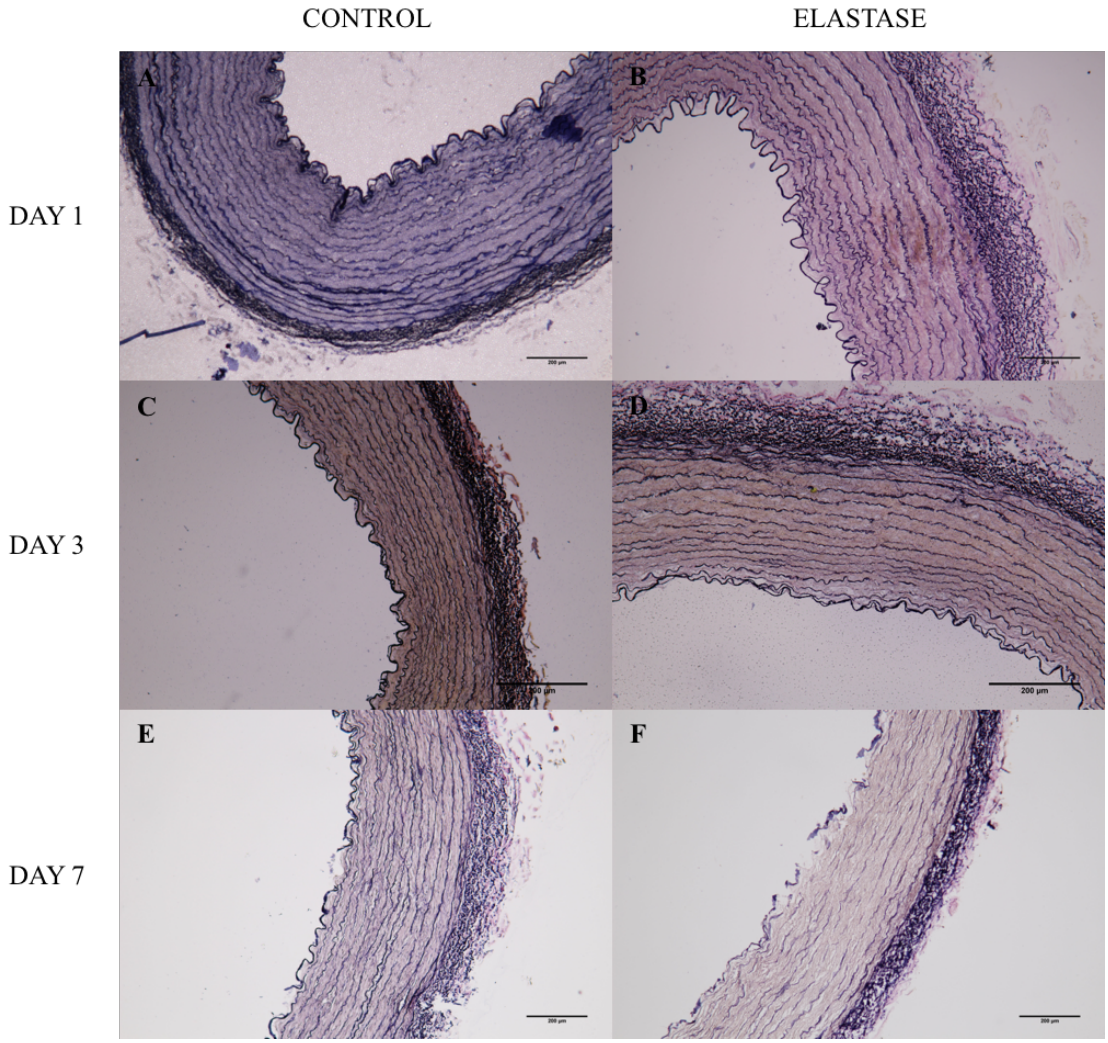

Figure 4.3: Verhoeff van Gieson (VVG) staining showing representative images (n = 3) of elastin damage in porcine carotid arteries after a 60 minute dosage of 20U elastase; (A) control, day 1; (B) elastase, day 1; (C) control, day 3; (D) elastase, day 3; (E) control, day 7; (F) elastase, day 7. 10x magnification.

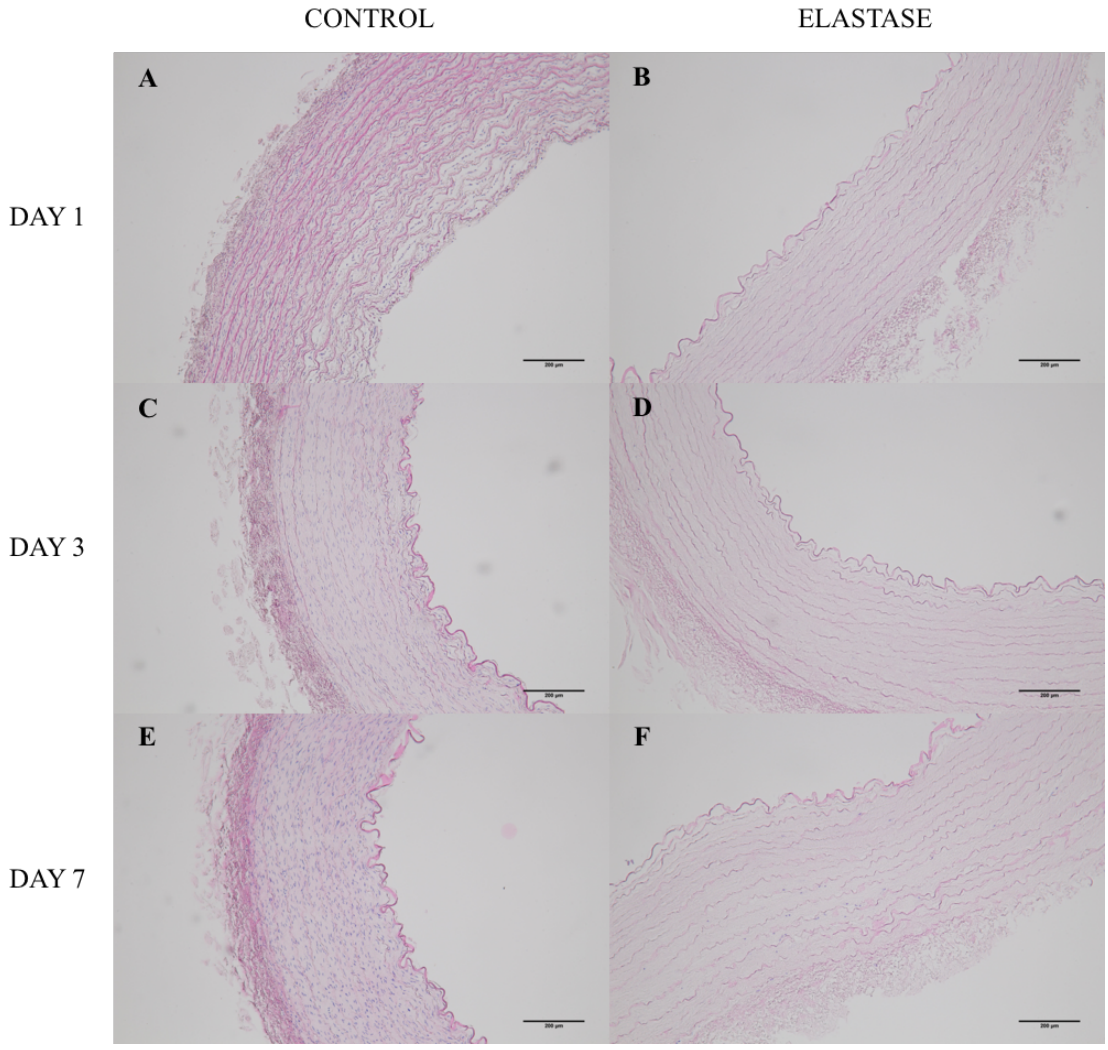

Figure 4.4: Hematoxylin and Eosin (H&E) staining showing representative images (n = 3) of cell death in porcine carotid arteries after a 60 minute dosage of 20U elastase; (A) control, day 1; (B) elastase, day 1; (C) control, day 3; (D) elastase, day 3; (E) control, day 7; (F) elastase, day 7. 10x magnification.

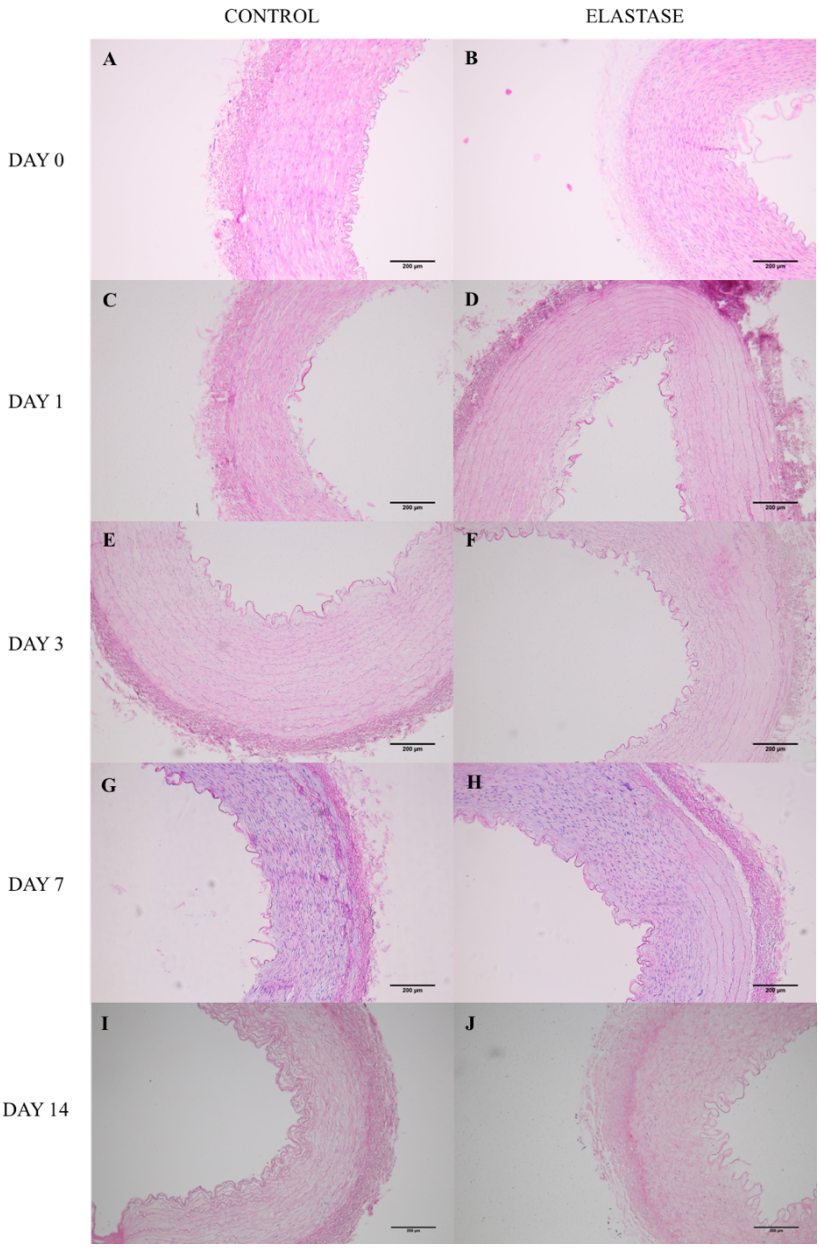

Figure 4.5: Hematoxylin and Eosin (H&E) staining showing representative images (n = 3) of cell migration patterns in porcine carotid arteries after a 15 minute dosage of 20U elastase; (A) control, day 0; (B) elastase, day 0; (C) control, day 1; (D) elastase, day 1; (E) control, day 3; (F) elastase, day 3; (G) control, day 7; (H) elastase, day 7; (I) control, day 14; (J) elastase, day 14. 10x magnification.

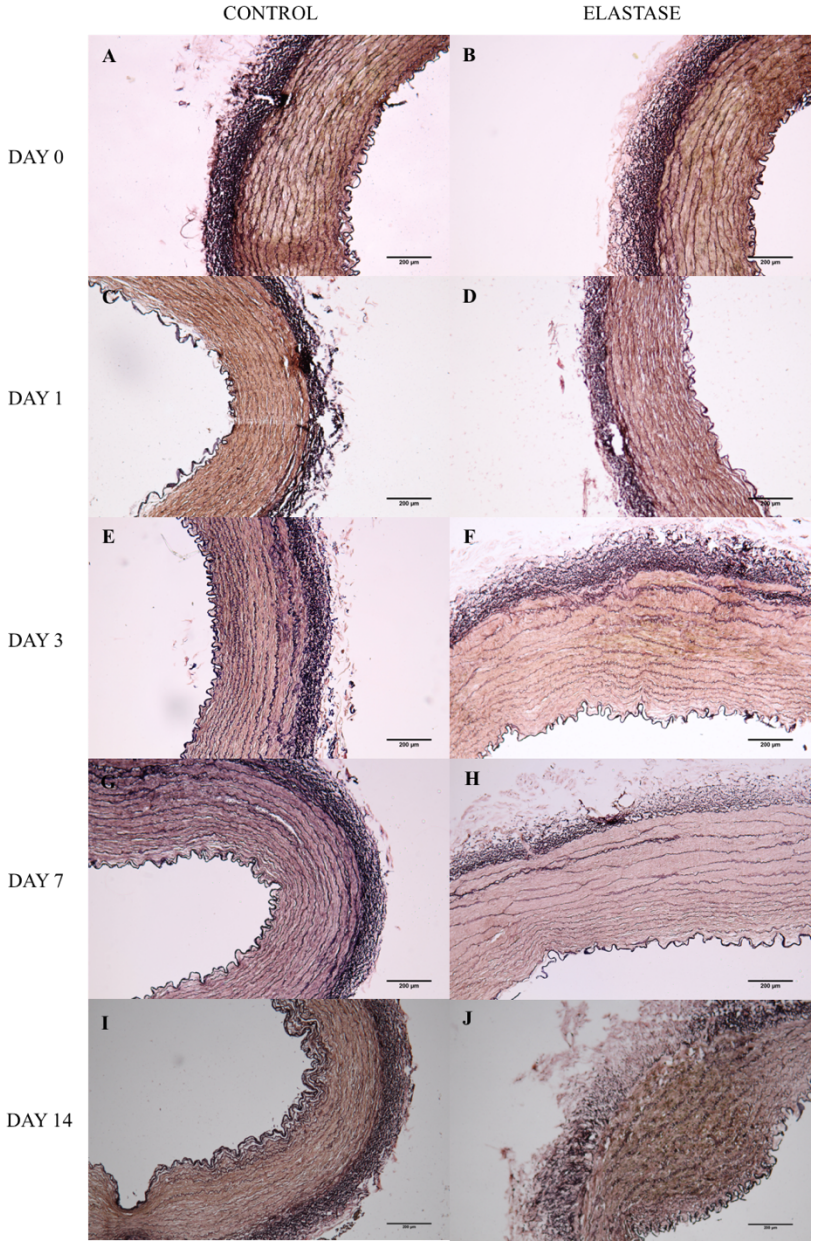

Figure 4.6: Verhoeff van Gieson staining showing representative images (n = 3) of elastin damage in porcine carotid arteries after a 15 minute dosage of 20U elastase; (A) control, day 0; (B) elastase, day 0; (C) control, day 1; (D) elastase, day 1; (E) control, day 3; (F) elastase, day 3; (G) control, day 7; (H) elastase, day 7; (I) control, day 14; (J) elastase, day 14. 10x magnification.

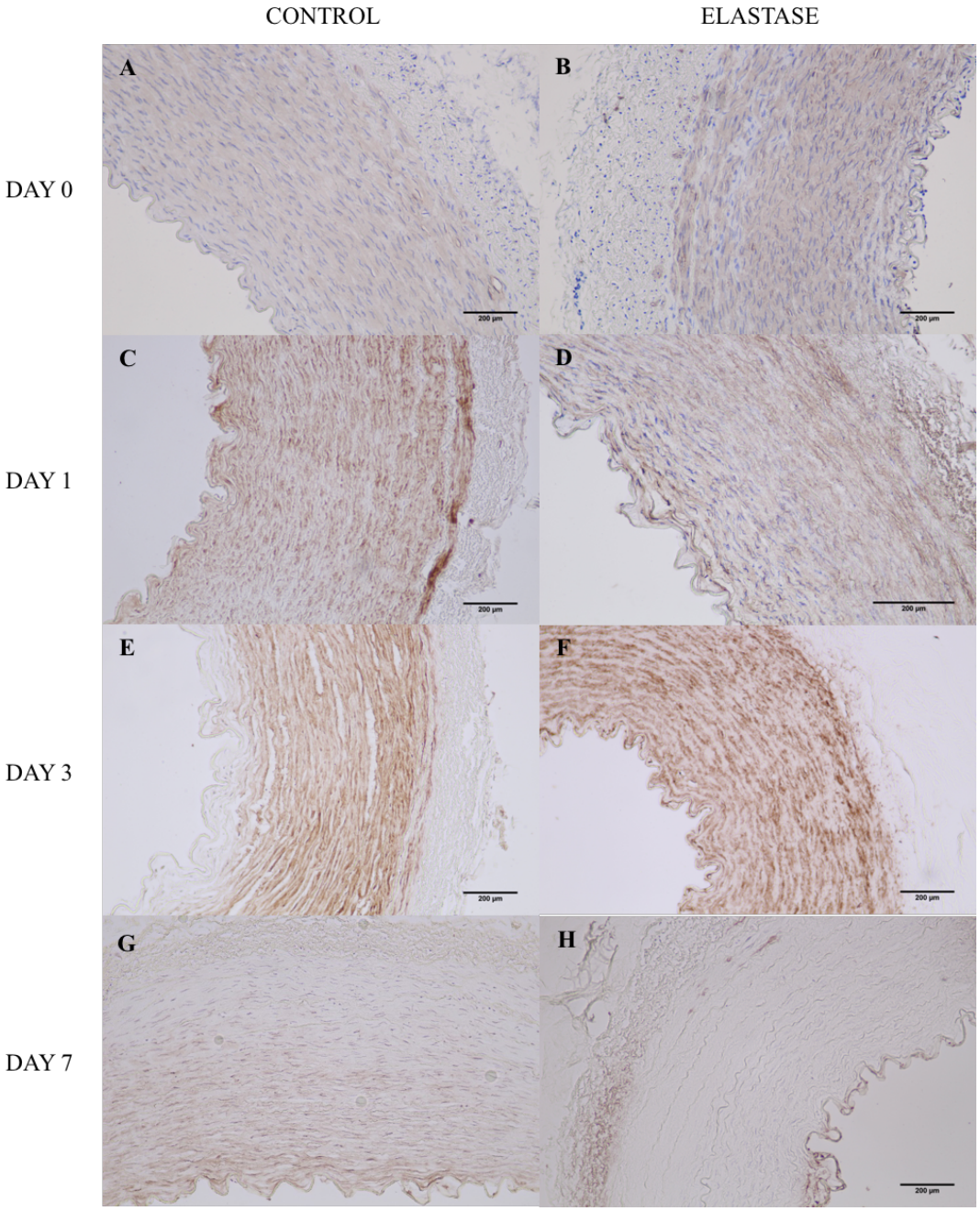

Figure 4.7: IHC for alpha smooth muscle actin showing representative images (n = 3) of VSMC loss in porcine carotid arteries after a 15 minute dosage of 20U elastase; (A) control, day 0; (B) elastase, day 0; (C) control, day 1; (D) elastase, day 1; (E) control, day 3; (F) elastase, day 3; (G) control, day 7; (H) elastase, day 7. 20x magnification.

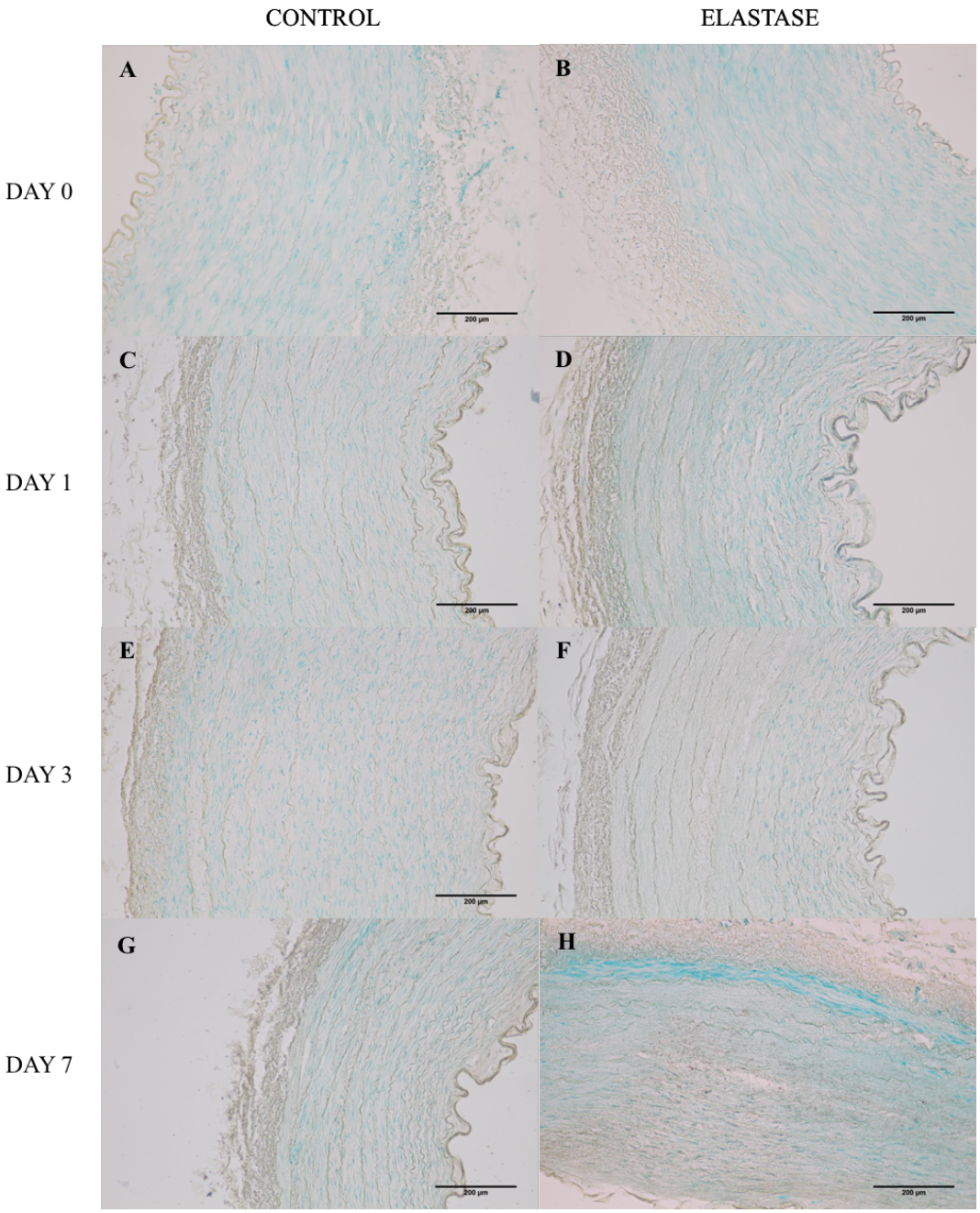

Figure 4.8: TUNEL assay showing representative images (n = 3) of apoptosis present in porcine carotid arteries after a 15 minute dosage of 20U elastase; (A) control, day 0; (B) elastase, day 0; (C) control, day 1; (D) elastase, day 1; (E) control, day 3; (F) elastase, day 3; (G) control, day 7; (H) elastase, day 7. 20x magnification.

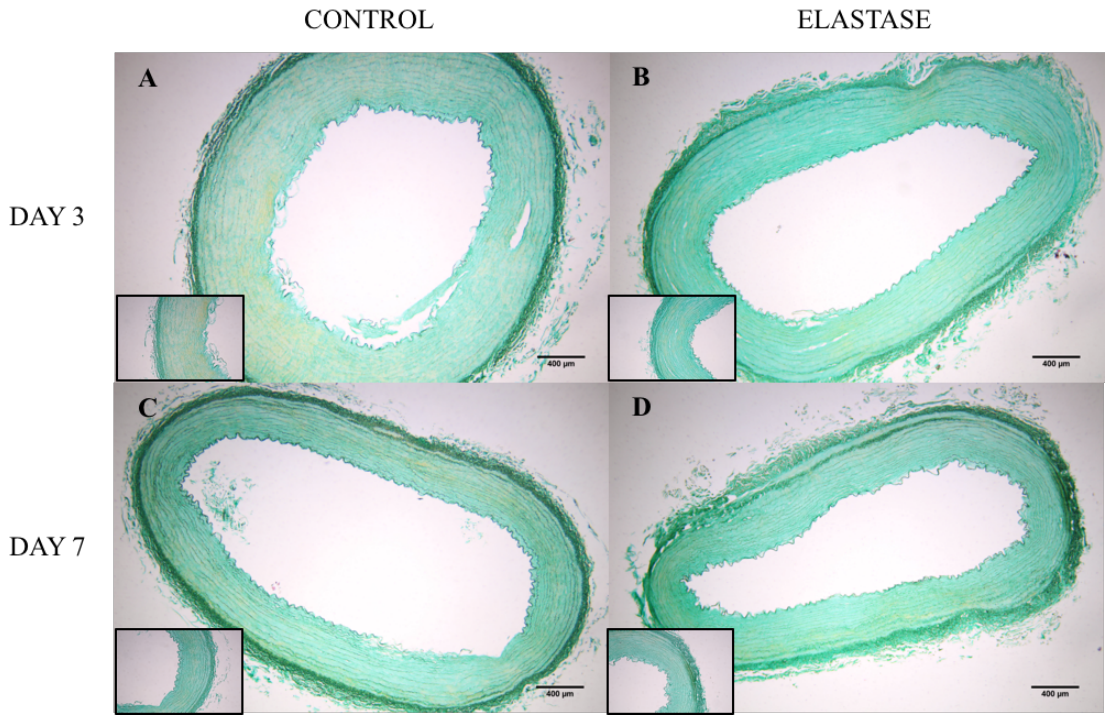

Figure 4.9: Alizarin red staining showing representative images (n = 3) of lack of calcification in porcine carotid arteries after a 15 minute dosage of 20U elastase; (A) control, day 3; (B) elastase, day 3; (C) control, day 7; (D) elastase, day 7. 4x magnification (10x magnification insert).

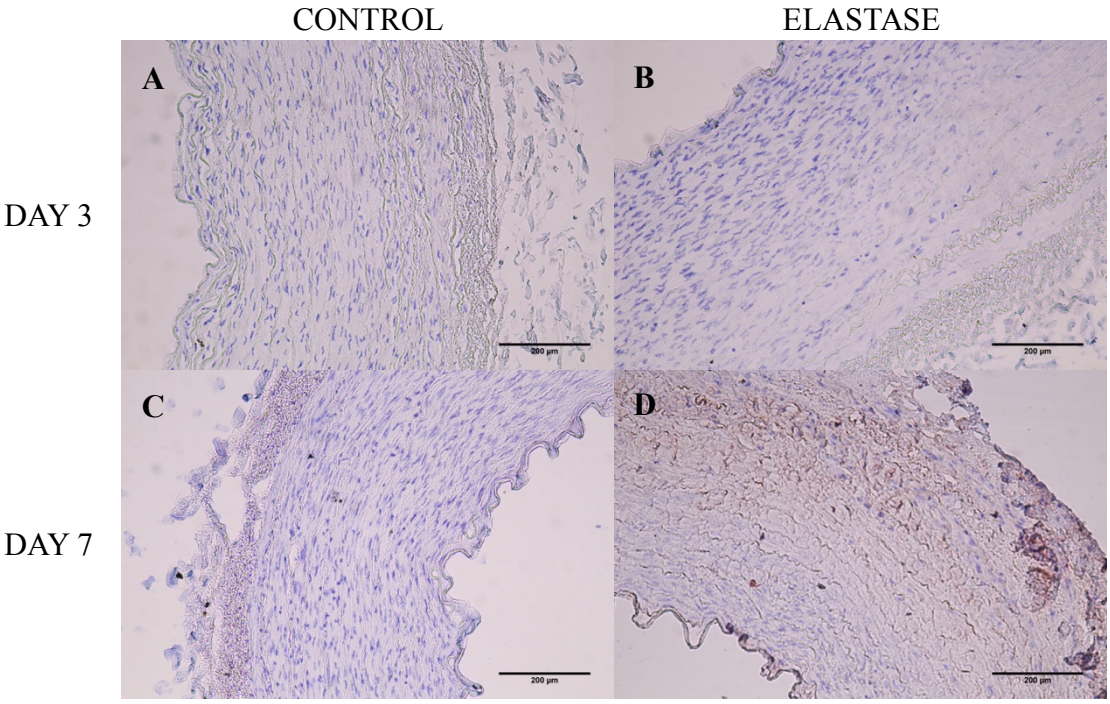

Figure 4.10: IHC for RUNX2 showing representative images (n = 3) of VSMC phenotypic switch to an osteogenic cell type present in porcine carotid arteries after a 15 minute dosage of 20U elastase; (A) control, day 3; (B) elastase, day 3; (C) control, day 7; (D) elastase, day 7. 20x magnification.

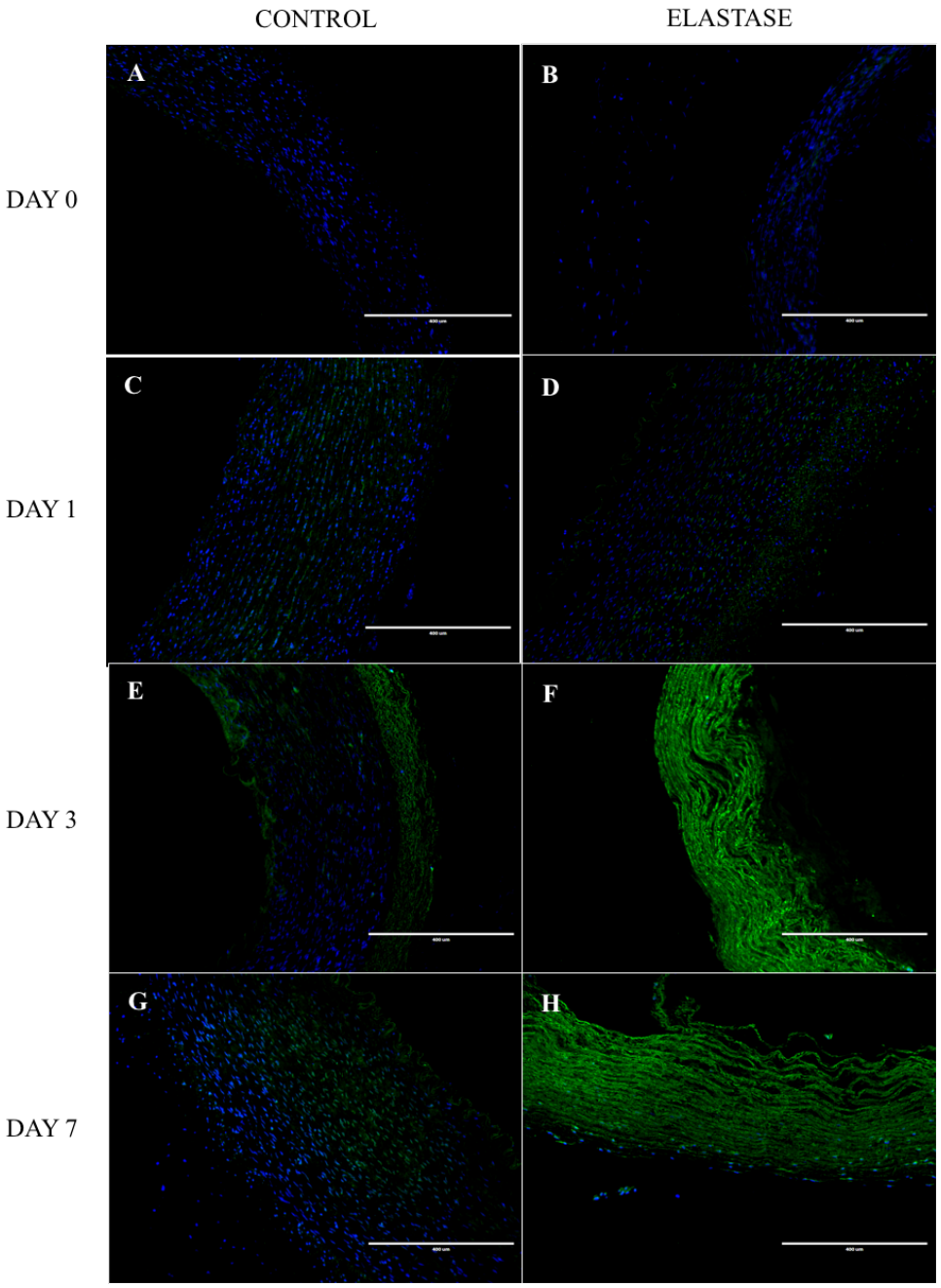

Figure 4.11: In situ zymography showing representative images (n = 3) of MMP activity present in porcine carotid arteries after a 15 minute dosage of 20U elastase; (A) control, day 0; (B) elastase, day 0; (C) control, day 1; (D) elastase, day 1; (E) control, day 3; (F) elastase, day 3; (G) control, day 7; (H) elastase, day 7. 20x magnification.

4.3 MMP Analysis

A FRET (Fluorescence resonance energy transfer) analysis was conducted using the substrate specific for both MMP-2 and MMP-9, the matrix metalloproteinases associated with AAA. Increased RFU (relative fluorescence units) is associated with increased presence of these MMPs. There was a statistically significant difference ($p < 0.05$) in the presence of MMPs in the elastase treated group at day 3 and day 7 when compared to the elastase time control at day 0 (Figure 4.12). There was also a statistically significant difference between the elastase treated groups at day 1 and day 3. The day 3 elastase treated samples also showed a statistically significant difference when compared to the control, untreated samples at the same time point. The largest amount of activity was seen in the day 3 elastase treated group, followed by the day 7 elastase treated group, which was consistent with the in situ zymography results (Table 4.1).

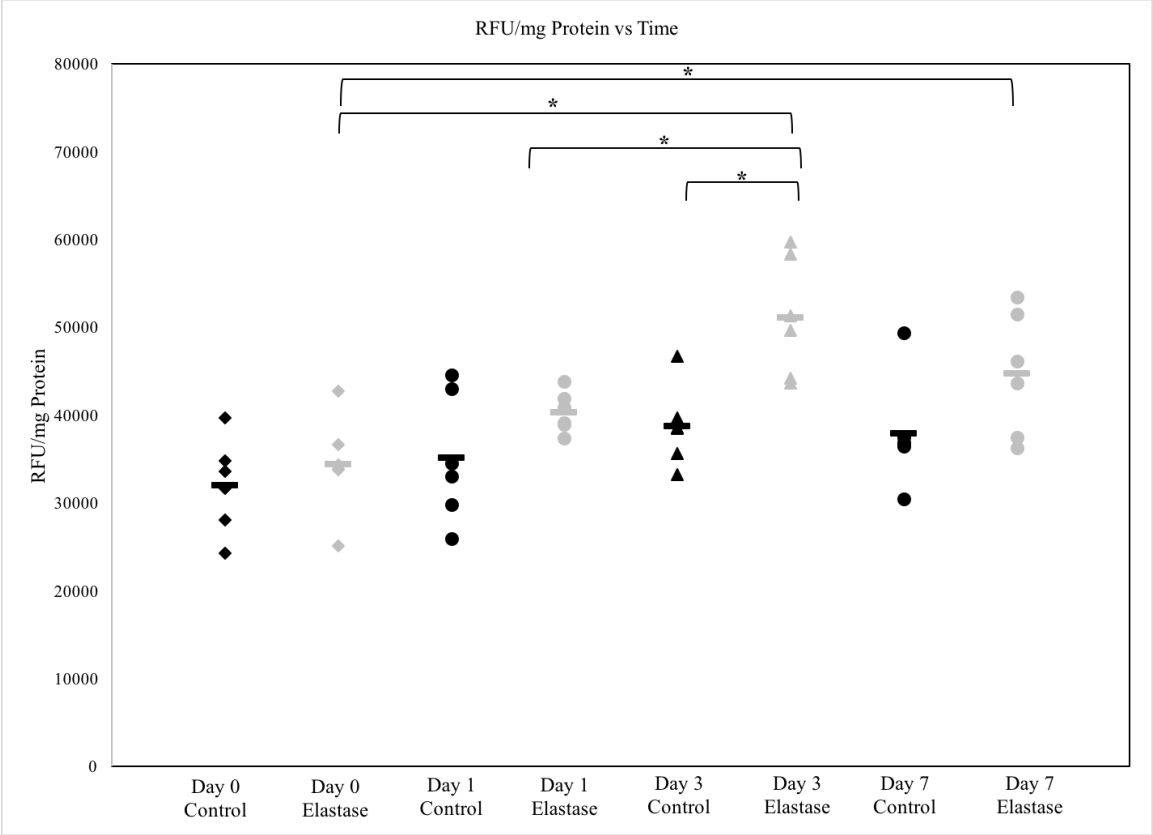

Figure 4.12: MMP presence as represented by RFU/mg protein of tissue; (n=6: dashes indicate mean values, * indicates statistically significant difference ($p < 0.05$)).

Group	RFU/mg protein
Day 0 Control	32001.15
Day 0 Elastase	34377.52
Day 1 Control	35110.49
Day 1 Elastase	40309.18
Day 3 Control	38687.70
Day 3 Elastase	51107.73
Day 7 Control	37858.69
Day 7 Elastase	44721.79

Table 4.1: MMP presence as represented by RFU/mg protein of tissue; (n = 6)

4.4 Desmosine Content

Desmosine content (ng desmosine/mg dry tissue weight) was determined using a porcine desmosine ELISA kit (MyBioSource, San Diego, CA). There was a statistically significant difference ($p < 0.05$) in the elastase treated group at day 0, the elastase treated group at day 3, and the elastase treated group at day 7. Elastase treated groups showed decreased desmosine content. This decrease in desmosine content showed progressive elastin degradation over time. Additionally, the results showed the decrease in desmosine content in the day 3 elastase treated groups is statistically significant ($p < 0.05$) when compared to control groups at day 1 and day 3, confirming that elastin damage is occurring

in the elastase treated groups relative to the control groups. The desmosine concentration in the control groups also decreased over time. This could be due to the continual degradation of ECM in organ culture. (Figure 4.13 and Table 4.2).

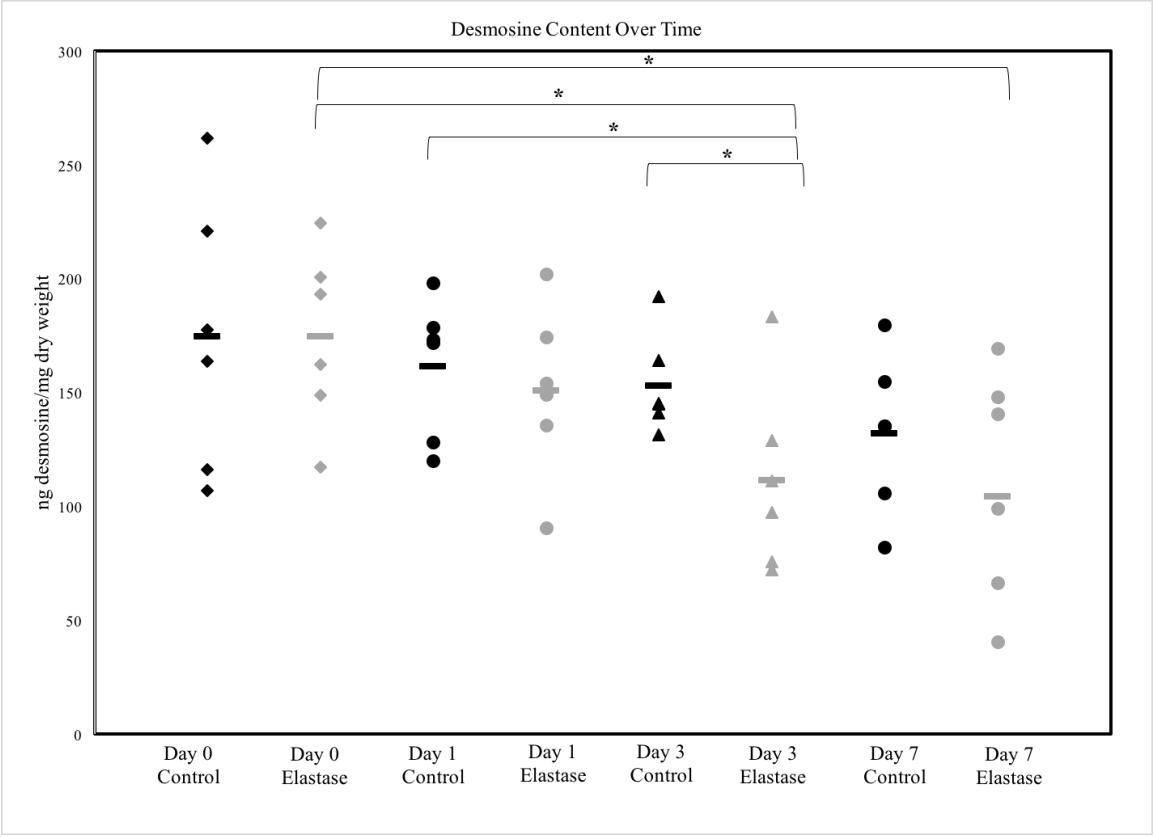

Figure 4.13: Desmosine content in samples represented by ng desmosine/mg dry tissue weight; (n = 6; * indicates statistically significant difference ($p < 0.05$)).

Group	Desmosine [ng]/dry weight tissue [mg]
Day 0 Control	174.48
Day 0 Elastase	174.53
Day 1 Control	161.66
Day 1 Elastase	150.99
Day 3 Control	153.32
Day 3 Elastase	111.44
Day 7 Control	132.21
Day 7 Elastase	110.74

Table 4.2: Desmosine content in samples represented by ng desmosine/mg dry tissue weight; (n = 6).

CHAPTER FIVE

DISCUSSION

AAA affects 1.7-12.7% of Americans and is currently the 13th leading cause of death in the United States[3,38]. Current treatments are suggested based on the risk of rupture, however surgical treatments remain risky and often require reintervention[59]. Conservative management of small aneurysms can also be deadly, as some research has shown that the risk of rupture may not be related to the size of the aneurysm. In order to further research into possible AAA treatments, a reliable large animal organ culture model must be established. The model should first optimize the concentration and dosage time of elastase to induce elastin damage as well as preserve cell life. Additionally, this model should show the progressive nature of the pathophysiology of AAA along with showing elastin damage, VSMC apoptosis, and presence of MMPs consistent with AAA. In order to accomplish this, a progressive organ culture model of AAA was investigated via elastase dosage in porcine carotid arteries[79,80,81,82,83,84,85,86,87].

5.1 Elastase Optimization

Initial attempts were made to determine how increasing concentrations of elastase affect elastin damage at a single time point. VVG staining showed that increasing concentrations (50U, 60U, and 80U) of PPE all applied for 10 minutes did not show an obvious change in elastin damage. From this, it was inferred that the focus should shift

towards evaluating how and increased dosage time would affect the elastin fibers. From this, lower concentrations (10U and 20U) of PPE were applied at increasing time points (20 minutes, 40 minutes, and 60 minutes) to determine how the length of elastase dosage affects elastin damage. Lower concentrations were used in the hopes of preventing excessive cell death that was believed would accompany higher concentrations of elastase for these lengthier time points. While there was elastin damage seen with a 20U dosage of elastase for 60 minutes, H&E staining of the same samples revealed that there was an overwhelming amount of cell death, making a 20U dose for 60 minutes an unviable option for this model.

The use of 20U of PPE for 15 minutes was found to be the elastase dosage that worked to insure elastin damage, as well as minimize cell death and was the concentration and dosage time used for this model.

5.2 Tissue Structure

5.2.1 Cell Migration

H&E staining showed cell migration away from the adventitial part of the artery, where the elastase was applied, towards the lumen beginning at day 1 in the elastase treated groups and is not seen in the control groups. Though the histology does show that the cells appear to be less abundant in these groups, the TUNEL assay revealed no apoptosis in the elastase treated groups, except in the day 7 group, which is consistent with VSMC apoptosis associated with AAA formation. This suggests that the cells are not dying, but

are migrating away from the adventitial dose of elastase with no remarkable effects on the outcome of the study or excessive cell death. There was remarkable cell death seen in the elastase treated group after 14 days, so the study was proceeded using time points of 0, 1, 3, and 7 days.

5.2.2 Elastin

Elastin fibers in the ECM are important to provide recoil for blood vessels. Elastin is cross-linked by lysine residues, as well as two amino acids specific to elastin, desmosine and isodesmosine, imparting integrity to the elastin fibers[33,34]. In the arteries, elastic fibers are organized into rings within the lumen[30]. Damage to elastin in AAA is due to the production of proteases with elastase activity by resident vascular cells within the artery, weakening the arterial wall, and forming AAA[3]. Elastin is degraded by proteases with elastase activity; this can be mimicked in animal models using porcine pancreatic elastase.

VVG staining showed fewer elastin fibers present in the elastase treated groups at day 3 and day 7 compared to time-matched controls and days 0 and 1 elastase treated groups, suggesting a model of AAA in the day 3 and day 7 groups. This decrease in elastin content shown in VVG is consistent with other progressive organ culture models, showing a decrease in elastin fiber content over time histologically[87].

Elastin damage can further be quantified by measuring desmosine content. As a cross-linking amino acid specific to elastin, a reduction in desmosine content within the tissue suggests elastin damage within the ECM. We were able to show a significant reduction in desmosine content in the day 3 elastase group (111.44 ng desmosine/mg dry

tissue weight) and the day 7 elastase group (110.74 ng desmosine/mg dry tissue weight) compared to the day 0 elastase group (174.53 ng desmosine/mg dry tissue weight), showing the progressive nature of this model in lowering the amount of desmosine in the tissue over time. Additionally, there was a statistically significant difference in the day 3 control and day 3 elastase treated groups (153.32 ng desmosine/mg dry tissue weight vs. 111.44 ng desmosine/mg dry tissue weight), suggesting significant elastin damage that could be consistent with AAA formation.

Of note, the weight of desmosine in the control samples did seem to decrease slightly over time. It is important to note that even though there was a decrease over time in the amount of desmosine present in the control groups, none of these decreases were statistically significant. This suggests that there could be some level of degradation of ECM in the organ culture.

5.2.3 VSMC Apoptosis

Diminished presence of VSMCs are thought to have implications in repair of the ECM during AAA formation, as they have roles in matrix synthesis, recruitment of inflammatory cells, and controlling proteases [50,51,52,53,55]. VSMCs are also associated with MMP-9 synthesis, increasing the amount of MMP-9 activation in AAA[55]. VSMC apoptosis is thought to be associated with degradation of the tunica media in this pathological process[88].

Our organ culture model showed a significant decrease in VSMC in the day 7 elastase treated group. This is shown histologically in IHC staining for alpha smooth

muscle actin and in the TUNEL assay, showing cell apoptosis in the day 7 elastase treated group that was not seen in time-matched controls.

The presence of diminished VSMCs in the tissue shown in IHC staining along with apoptosis present in the TUNEL assay is consistent with previous studies in AAA formation, suggesting that this marker consistent with AAA formation is present in this model[89,90].

5.2.4 Vascular Calcifiation

VSMC apoptosis is also associated with vascular calcification, as apoptotic blebs form and are able to collect calcium in a crystalized form[56]. Staining for calcification via Alizarin red showed no calcification in the day 3 and day 7 samples, however IHC staining for RUNX2, a transcription factor associated with osteoblast differentiation and one of the first markers of VSMC phenotypic switch to an osteogenic cell type was shown in the day 7 elastase treated group. This positive result suggests that the VSMCs in the day 7 elastase treated group are undergoing a phenotypic switch to an osteogenic cell type.

5.2.5 MMP Presence

The presence of MMP-2 and MMP-9 is frequently associated with AAA, as they are both implicated in the degradation of collagen and elastin[51,53]. MMP-2 and MMP-9 are both secreted by resident VSMCs.

The results of in situ zymography for MMP-2 and MMP-9 show the presence of MMP-2 and MMP-9 in the day 3 and day 7 elastase treated groups when compared to time

matched controls, consistent with the pathophysiology associated with AAA. Additionally, the increase in the presence of MMP-2 and MMP-9 is not seen in the day 0 and day 1 elastase treated groups, suggesting the progressive nature of this model, as the proteases become active in the later time points. The in situ zymography results showing fluorescence due to MMP presence are consistent with previous in situ zymography results published in AAA animal models[81].

In order to provide additional quantitative evidence of MMP presence in the samples, a FRET analysis was conducted. Consistent with the in situ zymography, a significant increase in MMP presence was seen in the day 3 (51107.73 RFU/mg protein) and day 7 (44721.79 RFU/mg protein) elastase treated groups when compared to the elastase treated group at day 0 (34377.52 RFU/mg protein).

There was little variation and no statistically significant difference in any of the control groups, suggesting consistency in the lack of MMP production in control samples. Though the day 7 elastase samples showed a decreased presence of MMP when compared to the day 3 elastase samples, there was no significant difference in the day 7 elastase group and time matched control, while there was a significant difference in the day 3 samples compared to the time matched control.

The decrease in MMP presence from day 3 to day 7 can be contributed to VSMC apoptosis. IHC for alpha smooth muscle actin and the TUNEL assay showed significant apoptosis of VSMC in the day 7 elastase group compared to the day 3 elastase group. Since VSMCs secrete MMPs, the apoptosis of VSMCs in day 7 accounts for the decrease in MMP presence seen in the in situ zymography and the FRET analysis.

5.3 Mechanism of Progressive Elastin Damage

Porcine pancreatic elastase (PPE) serine protease that was used to break down elastin[77]. PPE is inactive in the pancreas and is activated by trypsin when secreted into the intestines[77]. Elastin damage initiating aneurysm formation in animals in induced first by the loss of elastin fibers from the PPE perfusion, followed by continued damage due to an inflammatory response[78]. In the beginning days of this model, the elastin fibers become fragmented, followed by formation of a thrombus that accelerates AAA growth due to the activation and recruitment of MMP-2 and MMP-9[78].

Because this model was not an in vivo model, the typical extent of an inflammatory response did not occur. The progressive nature of this model is a result of the formation of elastin peptides formed during elastin fiber damage initiated by elastase, producing elastin peptides that act on the elastin-laminin receptor on the resident VSMCs, causing these VSMCs to become more inflammatory and furthering vessel damage and AAA pathogenesis[91,92].

CHAPTER SIX

CONCLUSIONS AND RECOMMENDATIONS

6.1 Conclusions

AAA is currently the 13th cause of death in the United States. Current surgical treatments for AAA are risky and invasive. Additionally, conservative measures can become deadly due to the dissenting information regarding AAA rupture mechanisms. Research into alternative treatment methods is abundant, particularly in small animal models, however there lacks a suitable organ culture model to replicate AAA for research to continue.

The results of this study show a promising organ culture model of AAA to fit this need. Elastase was used to degrade elastin fibers initiating the development of AAA. The progressive nature of this model is a result of the elastase-induced release of elastin peptides from elastin fibers[91]. These elastin fibers were then able to interact with the 67 kDa elastin-laminin receptor on the resident VSMCs, causing these cells to become more inflammatory and further the pathogenesis of AAA[92]. This study showed elastin degradation histologically, as well as through a decrease in desmosine content to provide evidence of elastin degradation consistent with AAA. Additionally, the decrease in VSMC concentration and prevalence of VSMC apoptosis in the day 7 elastase treated group shown are also present in AAA pathophysiology. While this VSMC apoptosis at day 7 does not show any associated calcification at that time point, histology does show the presence of

transcription factors associated with VSMC phenotypic switch to a more osteogenic cell type. Additionally, analysis of MMPs showed their presence in the day 3 and day 7 elastase treated group providing further evidence of a successful model of AAA. The slight decrease in MMP presence in the day 7 elastase treated group compared to the day 3 elastase treated group is due to the VSMC apoptosis shown in the day 7 elastase treated group, as VSMCs are responsible for MMP production; therefore, a reduction in VSMCs results in a reduction in MMPs. Lastly, the elastase dosage was optimized to prevent excessive cell death to recapitulate an in vivo response.

While the day 3 and day 7 elastase treated groups both showed markers consistent with AAA, the day 7 group shows additional promise in further research due to possible VSMC phenotypic switches that should be further investigated.

Thus, we have successfully shown a progressive model of AAA formation. This model provides evidence of important pathological markers present in AAA including elastin degradation, VSMC apoptosis, and MMP production.

6.2 Limitations

Despite the success of this model previously described, there are limitations to be considered. Because this model is performed ex vivo, the inflammatory response associated with AAA was unable to be replicated in this model as it would occur in an in vivo model. Additionally, this model was performed in static culture and did not replicate blood flow through the vessels as it would occur in the human body.

6.3 Recommendations

This study has demonstrated a successful organ culture model of AAA formation by characterizing basic pathological responses consistent with AAA. Future work should include long term studies to investigate the VSMC phenotypic switches. Experiments should be performed to determine if there is an increase in BMP or alkaline phosphatase and formation of calcium deposits. This will provide additional insight to the relationship between vascular calcification and AAA.

Additionally, performing this study in perfusion culture could provide valuable insight into how fluid flow affects the results of this study, as perfusion culture would more mimic blood flow through the arteries in humans. Furthermore, as high blood pressure is strongly associated with AAA, perfusion culture would also allow the ability for the vessel to be pressurized in order to mimic the conditions of those with hypertension. From this, the effects of high blood pressure could be established.

As mentioned previously, a limitation to this model is its inability to fully capture the inflammatory response associated with AAA as it would occur in an in vivo model. Incorporating inflammatory cells like macrophages and cytokines associated with this response would provide a more realistic model of this disease.

REFERENCES

1. Kumar, Y. *et al.* Abdominal aortic aneurysm: pictorial review of common appearances and complications. *Ann Transl Med* **5**, (2017).
2. Aggarwal, S., Qamar, A., Sharma, V. & Sharma, A. Abdominal aortic aneurysm: A comprehensive review. *Exp Clin Cardiol* **16**, 11–15 (2011).
3. Sakalihasan, N., Limet, R. & Defawe, O. D. Abdominal aortic aneurysm. **365**, 13 (2005).
4. Klaus, V. *et al.* Association of Matrix Metalloproteinase Levels with Collagen Degradation in the Context of Abdominal Aortic Aneurysm. *Eur J Vasc Endovasc Surg* **53**, 549–558 (2017).
5. Rodella, L. F. *et al.* Abdominal aortic aneurysm and histological, clinical, radiological correlation. *Acta Histochem.* **118**, 256–262 (2016).
6. Anidjar, S. *et al.* Elastase-induced experimental aneurysms in rats. *Circulation* **82**, 973–981 (1990).
7. Tsui, J. C. Experimental Models of Abdominal Aortic Aneurysms. *Open Cardiovasc Med J* **4**, 221–230 (2010).
8. Heart Disease Facts & Statistics | cdc.gov. (2018). Available at: https://www.cdc.gov/heartdisease/facts.htm. (Accessed: 3rd June 2019)
9. Underlying Cause of Death 1999-2017. Available at: https://wonder.cdc.gov/wonder/help/ucd.html. (Accessed: 3rd June 2019)

10. Aortic Aneurysm Fact Sheet|Data & Statistics|DHDSP|CDC. (2018). Available at: https://www.cdc.gov/dhdsp/data_statistics/fact_sheets/fs_aortic_aneurysm.htm. (Accessed: 3rd June 2019)

11. Heart Disease and Stroke Statistics—2013 Update | Circulation. Available at: https://www.ahajournals.org/doi/full/10.1161/CIR.0b013e31828124ad. (Accessed: 3rd June 2019)

12. Pugsley, M. K. & Tabrizchi, R. The vascular system An overview of structure and function. *Journal of Pharmacological and Toxicological Methods* 8 (2000).

13. Borysenko: Functional histology - Google Scholar. Available at: https://scholar.google.com/scholar_lookup?title=Functional%20histology&publication_year=1984&author=M.%20Borysenko&author=T.%20Beringer. (Accessed: 18th April 2019)

14. Hirschi, K. K. Pericytes in the microvasculature. 12

15. Gray, H. *Anatomy of the Human Body*. (Lea & Febiger, 1878).

16. Isselbacher Eric M. Thoracic and Abdominal Aortic Aneurysms. *Circulation* **111**, 816–828 (2005).

17. Aorta: Aortic Aneurysm. *Cleveland Clinic* Available at: https://my.clevelandclinic.org/health/diseases/16742-aorta-aortic-aneurysm. (Accessed: 13th May 2019)

18. Hynes, R. O. The Extracellular Matrix: Not Just Pretty Fibrils. *Science* **326**, 1216–1219 (2009).

19. Frantz, C., Stewart, K. M. & Weaver, V. M. The extracellular matrix at a glance. *Journal of Cell Science* **123**, 4195–4200 (2010).

20. Schaefer, L. & Schaefer, R. M. Proteoglycans: from structural compounds to signaling molecules. *Cell Tissue Res* **339**, 237 (2009).

21. Rozario, T. & DeSimone, D. W. The Extracellular Matrix In Development and Morphogenesis: A Dynamic View. *Dev Biol* **341**, 126–140 (2010).

22. Shoulders, M. D. & Raines, R. T. Collagen Structure and Stability. *Annual Review of Biochemistry* **78**, 929–958 (2009).

23. Kadler, K. E., Holmes, D. F., Trotter, J. A. & Chapman, J. A. Collagen fibril formation. *Biochemical Journal* **316**, 1–11 (1996).

24. Lee, C. H., Singla, A. & Lee, Y. Biomedical applications of collagen. *International Journal of Pharmaceutics* **221**, 1–22 (2001).

25. van der Rest, M. & Garrone, R. Collagen family of proteins. *The FASEB Journal* **5**, 2814–2823 (1991).

26. Lodish, H. *et al.* Collagen: The Fibrous Proteins of the Matrix. *Molecular Cell Biology. 4th edition* (2000).

27. Trentham, D. E. Autoimmunity to type II collagen an experimental model of arthritis. *Journal of Experimental Medicine* **146**, 857–868 (1977).

28. Bächinger, H. P., Mizuno, K., Vranka, J. A. & Boudko, S. P. 5.16 - Collagen Formation and Structure. in *Comprehensive Natural Products II* (eds. Liu, H.-W. (Ben) & Mander, L.) 469–530 (Elsevier, 2010). doi:10.1016/B978-008045382-8.00698-5

29. Wise, S. G. & Weiss, A. S. Tropoelastin. *The International Journal of Biochemistry & Cell Biology* **41**, 494–497 (2009).

30. Mithieux, S. M. & Weiss, A. S. Elastin. in *Advances in Protein Chemistry* **70**, 437–461 (Academic Press, 2005).

31. Lucero, H. A. & Kagan, H. M. Lysyl oxidase: an oxidative enzyme and effector of cell function. *Cellular and Molecular Life Sciences* **63**, 2304–2316 (2006).

32. Debelle, L. & Tamburro, A. M. Elastin: molecular description and function. *The International Journal of Biochemistry & Cell Biology* **31**, 261–272 (1999).

33. Eyre, D. R., Paz, M. A. & Gallop, P. M. Cross-Linking in Collagen and Elastin. *Annual Review of Biochemistry* **53**, 717–748 (1984).

34. Anwar, R. A. Elastin: A brief Review. *Biochemical Education* **18**, 162–166 (1990).

35. Luisetti, M. *et al.* Desmosine as a biomarker of elastin degradation in COPD: current status and future directions. *European Respiratory Journal* **32**, 1146–1157 (2008).

36. Smith, M. L. *et al.* Force-Induced Unfolding of Fibronectin in the Extracellular Matrix of Living Cells. *PLoS Biol* **5**, (2007).

37. Trebaul, A., Chan, E. K. & Midwood, K. S. Regulation of fibroblast migration by tenascin-C. *Biochemical Society Transactions* **35**, 695–697 (2007).

38. Association of Matrix Metalloproteinase Levels with Collagen Degradation in the Context of Abdominal Aortic Aneurysm | Elsevier Enhanced Reader. doi:10.1016/j.ejvs.2016.12.030

39. Outcome of elective treatment of abdominal aortic aneurysm in elderly patients | Elsevier Enhanced Reader. doi:10.1016/j.ijsu.2015.02.001

40. Abdominal ultrasound of an abdominal aortic aneurysm. *Mayo Clinic* Available at: https://www.mayoclinic.org/tests-procedures/abdominal-ultrasound/multimedia/img-20149630. (Accessed: 19th April 2019)

41. Hannawa, K. K., Eliason, J. L. & Upchurch, G. R. Gender Differences in Abdominal Aortic Aneurysms. *Vascular* **17**, S30–S39 (2009).

42. Golledge, J. & Norman, P. Atherosclerosis and abdominal aortic aneurysm: Cause, response or common risk factors? *Arterioscler Thromb Vasc Biol* **30**, 1075–1077 (2010).

43. High Prevalence of Abdominal Aortic Aneurysm in Patients with Three-vessel Coronary Artery Disease | Elsevier Enhanced Reader. doi:10.1016/j.ejvs.2013.12.011

44. Shibamura, H. *et al.* Genome Scan for Familial Abdominal Aortic Aneurysm Using Sex and Family History as Covariates Suggests Genetic Heterogeneity and Identifies Linkage to Chromosome 19q13. *Circulation* **109**, 2103–2108 (2004).

45. Sofi, F. *et al.* High levels of homocysteine, lipoprotein (a) and plasminogen activator inhibitor-1 are present in patients with abdominal aortic aneurysm. *Thromb. Haemost.* **94**, 1094–1098 (2005).

46. Strauss, E., Waliszewski, K., Gabriel, M., Zapalski, S. & Pawlak, A. L. Increased risk of the abdominal aortic aneurysm in carriers of the MTHFR 677T allele. *J. Appl. Genet.* **44**, 85–93 (2003).

47. Jones, G. T., Harris, E. L., Phillips, L. V. & van Rij, A. M. The methylenetetrahydrofolate reductase C677T polymorphism does not associate with susceptibility to abdominal aortic aneurysm. *Eur J Vasc Endovasc Surg* **30**, 137–142 (2005).

48. Thompson, R. W. ATVB In Focus: Abdominal Aortic Aneurysms: Pathophysiological Mechanisms and Clinical Implications. *ATVB* **24**, 240–240 (2004).

49. Kuivaniemi, H., Ryer, E. J., Elmore, J. R. & Tromp, G. Understanding the pathogenesis of abdominal aortic aneurysms. *Expert Rev Cardiovasc Ther* **13**, 975–987 (2015).

50. Thompson, R. W. *et al.* Pathophysiology of Abdominal Aortic Aneurysms: Insights from the Elastase-Induced Model in Mice with Different Genetic Backgrounds. *Annals of the New York Academy of Sciences* **1085**, 59–73 (2006).

51. Guo, D.-C., Papke, C. L., He, R. & Milewicz, D. M. Pathogenesis of Thoracic and Abdominal Aortic Aneurysms. *Annals of the New York Academy of Sciences* **1085**, 339–352 (2006).

52. Sakalihasan, N., Delvenne, P., Nusgens, B. V., Limet, R. & Lapière, C. M. Activated forms of MMP2 and MMP9 in abdominal aortic aneurysms. *Journal of Vascular Surgery* **24**, 127–133 (1996).

53. Longo, G. M. *et al.* Matrix metalloproteinases 2 and 9 work in concert to produce aortic aneurysms. *J Clin Invest* **110**, 625–632 (2002).

54. Basalyga, D. M. *et al.* Elastin Degradation and Calcification in an Abdominal Aorta Injury Model. *Circulation* **110**, 3480–3487 (2004).

55. Airhart, N. *et al.* Smooth Muscle Cells from Abdominal Aortic Aneurysms are Unique and Can Independently and Synergistically Degrade Insoluble Elastin. *J Vasc Surg* **60**, 1033-1042.e5 (2014).

56. Proudfoot, D. *et al.* The role of apoptosis in the initiation of vascular calcification. *Z Kardiol* **90 Suppl 3**, 43–46 (2001).

57. Liu, J. *et al.* Cathepsin L expression and regulation in human abdominal aortic aneurysm, atherosclerosis, and vascular cells. *Atherosclerosis* **184**, 302–311 (2006).

58. Sukhova, G. K., Shi, G. P., Simon, D. I., Chapman, H. A. & Libby, P. Expression of the elastolytic cathepsins S and K in human atheroma and regulation of their production in smooth muscle cells. *J. Clin. Invest.* **102**, 576–583 (1998).

59. Wilt, T. J. *et al. Comparison of Endovascular and Open Surgical Repairs for Abdominal Aortic Aneurysm*. (Agency for Healthcare Research and Quality (US), 2006).

60. Sun, Z.-H. Abdominal aortic aneurysm: Treatment options, image visualizations and follow-up procedures. *J Geriatr Cardiol* **9**, 49–60 (2012).

61. Surgery for Abdominal Aortic Aneurysm. Available at: https://www.fairview.org/patient-education/82914. (Accessed: 2nd May 2019)

62. Davis, F. M., Rateri, D. L. & Daugherty, A. Abdominal Aortic Aneurysm: Novel Mechanisms and Therapies. *Curr Opin Cardiol* **30**, 566–573 (2015).

63. Joddar, B. & Ramamurthi, A. Fragment size- and dose-specific effects of hyaluronan on matrix synthesis by vascular smooth muscle cells. *Biomaterials* **27**, 2994–3004 (2006).

64. Joddar, B. & Ramamurthi, A. Elastogenic effects of exogenous hyaluronan oligosaccharides on vascular smooth muscle cells. *Biomaterials* **27**, 5698–5707 (2006).

65. Kothapalli, C. R., Taylor, P. M., Smolenski, R. T., Yacoub, M. H. & Ramamurthi, A. Transforming growth factor beta 1 and hyaluronan oligomers synergistically enhance elastin matrix regeneration by vascular smooth muscle cells. *Tissue Eng Part A* **15**, 501–511 (2009).

66. Kothapalli, C. R., Gacchina, C. E. & Ramamurthi, A. Utility of Hyaluronan Oligomers and Transforming Growth Factor-Beta1 Factors for Elastic Matrix Regeneration by Aneurysmal Rat Aortic Smooth Muscle Cells. *Tissue Eng Part A* **15**, 3247–3260 (2009).

67. Gacchina, C. E., Deb, P., Barth, J. L. & Ramamurthi, A. Elastogenic Inductability of Smooth Muscle Cells from a Rat Model of Late Stage Abdominal Aortic Aneurysms. *Tissue Engineering Part A* **17**, 1699–1711 (2011).

68. Swaminathan, G., Stoilov, I., Broekelmann, T., Mecham, R. & Ramamurthi, A. Phenotype-based selection of bone marrow mesenchymal stem cell-derived smooth muscle cells for elastic matrix regenerative repair in abdominal aortic aneurysms. *Journal of Tissue Engineering and Regenerative Medicine* **12**, e60–e70 (2018).

69. Swaminathan, G. *et al.* Pro-elastogenic effects of bone marrow mesenchymal stem cell-derived smooth muscle cells on cultured aneurysmal smooth muscle cells. *J Tissue Eng Regen Med* **11**, 679–693 (2017).

70. Sharma, A. K. *et al.* Mesenchymal Stem Cells Attenuate NADPH Oxidase-Dependent High Mobility Group Box 1 Production and Inhibit Abdominal Aortic Aneurysms. *Arterioscler Thromb Vasc Biol.* **36**, 908–918 (2016).

71. Davis, F. M., Daugherty, A. & Lu, H. S. Updates of Recent Aortic Aneurysm Research. *ATVB* **39**, (2019).

72. Daugherty, A. & Cassis, L. Angiotensin II-Mediated Development of Vascular Diseases. *Trends in Cardiovascular Medicine* **14**, 117–120 (2004).

73. Weintraub, N. L. Understanding Abdominal Aortic Aneurysm. *N Engl J Med* **361**, 1114–1116 (2009).

74. Daugherty, A., Rateri, D. L. & Cassis, L. A. Role of the Renin-Angiotensin System in the Development of Abdominal Aortic Aneurysms in Animals and Humans. *Annals of the New York Academy of Sciences* **1085**, 82–91 (2006).

75. The calcium chloride-induced rodent model of abdominal aortic aneurysm | Elsevier Enhanced Reader. doi:10.1016/j.atherosclerosis.2012.09.010

76. Annambhotla, S. *et al.* Recent Advances in Molecular Mechanisms of Abdominal Aortic Aneurysm Formation. *World J Surg* **32**, 976–986 (2008).

77. Human leukocyte and porcine pancreatic elastase: x-ray crystal structures, mechanism, substrate specificity, and mechanism-based inhibitors. Available at: https://pubs.acs.org/doi/pdf/10.1021/bi00431a001. (Accessed: 13th May 2019)

78. Sénémaud, J. *et al.* Translational Relevance and Recent Advances of Animal Models of Abdominal Aortic Aneurysm. *Arterioscler Thromb Vasc Biol.* **37**, 401–410 (2017).

79. Nosoudi, N. *et al.* Systemic Delivery of Nanoparticles Loaded with Pentagalloyl Glucose Protects Elastic Lamina and Prevents Abdominal Aortic Aneurysm in Rats. *J. of Cardiovasc. Trans. Res.* **9**, 445–455 (2016).

80. Yoshimura, K. *et al.* Current Status and Perspectives on Pharmacologic Therapy for Abdominal Aortic Aneurysm. *Curr Drug Targets* **19**, 1265–1275 (2018).

81. Nosoudi Nasim *et al.* Prevention of Abdominal Aortic Aneurysm Progression by Targeted Inhibition of Matrix Metalloproteinase Activity With Batimastat-Loaded Nanoparticles. *Circulation Research* **117**, e80–e89 (2015).

82. Wang, Q. *et al.* Receptor-interacting protein kinase 3 contributes to abdominal aortic aneurysms via smooth muscle cell necrosis and inflammation. *Circ. Res.* **116**, 600–611 (2015).

83. Wang, Q. *et al.* Inhibition of Receptor-Interacting Protein Kinase 1 with Necrostatin–1s ameliorates disease progression in elastase-induced mouse abdominal aortic aneurysm model. *Sci Rep* **7**, (2017).

84. Pope, N. H. *et al.* D-series resolvins inhibit murine abdominal aortic aneurysm formation and increase M2 macrophage polarization. *FASEB J* **30**, 4192–4201 (2016).

85. Pillai, P. S. *et al.* Chemical Mediators of Inflammation and Resolution in Post-Operative Abdominal Aortic Aneurysm Patients. *Inflammation* **35**, 98–113 (2012).

86. Harada Takasuke *et al.* Focal Adhesion Kinase Promotes the Progression of Aortic Aneurysm by Modulating Macrophage Behavior. *Arteriosclerosis, Thrombosis, and Vascular Biology* **37**, 156–165 (2017).

87. Wills, A. *et al.* Elastase-induced matrix degradation in arterial organ cultures: An in vitro model of aneurysmal disease. *Journal of Vascular Surgery* **24**, 667–679 (1996).

88. Rowe, V. L. *et al.* Vascular smooth muscle cell apoptosis in aneurysmal, occlusive, and normal human aortas. *Journal of Vascular Surgery* **31**, 567–576 (2000).

89. López-Candales, A. *et al.* Decreased vascular smooth muscle cell density in medial degeneration of human abdominal aortic aneurysms. *Am J Pathol* **150**, 993–1007 (1997).

90. Henderson, E. L. *et al.* Death of Smooth Muscle Cells and Expression of Mediators of Apoptosis by T Lymphocytes in Human Abdominal Aortic Aneurysms. *Circulation* **99**, 96–104 (1999).

91. de Oliveira, E. B. & Salgado, M. C. O. Chapter 584 - Pancreatic Elastases. in *Handbook of Proteolytic Enzymes (Third Edition)* (eds. Rawlings, N. D. & Salvesen, G.) 2639–2645 (Academic Press, 2013). doi:10.1016/B978-0-12-382219-2.00584-6

92. Faury, G. Role of the elastin-laminin receptor in the cardiovascular system. *Pathol. Biol.* **46**, 517–526 (1998).